One-loop amplitudes for $t\bar{t}j$ and $t\bar{t}\gamma$ productions at the LHC through $\mathcal{O}(\epsilon^2)$

Souvik Bera[1]♣, Colomba Brancaccio[2]♡, Dhimiter Canko[3]♠ and Heribertus Bayu Hartanto[1,4]◇

1 Asia Pacific Center for Theoretical Physics, Pohang, 37673, Korea
2 Dipartimento di Fisica and Arnold-Regge Center, Università di Torino, and INFN, Sezione di Torino, Via P. Giuria 1, I-10125 Torino, Italy
3 Dipartimento di Fisica e Astronomia, Università di Bologna e INFN, Sezione di Bologna, via Irnerio 46, I-40126 Bologna, Italy
4 Department of Physics, Pohang University of Science and Technology, Pohang, 37673, Korea

♣ souvik.bera@apctp.org , ♡ colomba.brancaccio@unito.it , ♠ dhimiter.canko2@unibo.it ,
◇ bayu.hartanto@apctp.org

Abstract

We present analytic expressions for the one-loop QCD helicity amplitudes contributing to top-quark pair production in association with a photon or a jet at the Large Hadron Collider (LHC), evaluated through $\mathcal{O}(\epsilon^2)$ in the dimensional regularisation parameter, ϵ. These amplitudes are required to construct the two-loop hard functions that enter the NNLO QCD computation. The helicity amplitudes are expressed as linear combinations of algebraically independent components of the ϵ-expanded master integrals–known as pentagon function–with the corresponding rational coefficients written in terms of momentum-twistor variables. We derive differential equations for the pentagon functions and solve them numerically using the generalised power series expansion method.

Contents

1   Introduction

The top-quark sector of the Standard Model of particle physics (SM) has been extensively studied at hadron collider experiments, providing stringent tests of the SM and offering a window into the exploration of Beyond the Standard Model (BSM) mechanisms [1–4]. In contrast to other strongly interacting particles in the SM, the top quark has the unique property of decaying before forming an hadronic bound state, a consequence of its large mass and short lifetime. As a result, its decay products not only provide direct access to the study of the top-quark properties, but also retain information through spin correlations, which persist because of the short decay time. Top-quark pair production in association with an additional particle, such as a jet ($t\bar{t}j$), a Higgs boson ($t\bar{t}H$), or a vector boson ($t\bar{t}V$, where $V \in \{\gamma, W^{\pm}, Z\}$), warrants a wide range of phenomenological investigations, due to the rich kinematics of $2 \to 3$ scattering processes.

In this article, we focus on processes involving top-quark pair production in association with a massless particle, specifically $pp \to t\bar{t}j$ and $pp \to t\bar{t}\gamma$. The $t\bar{t}\gamma$ production mechanism provides direct access to measure the top-quark charge [5] and allows to probe the structure of the top-photon vertex [6, 7] within the Standard Model Effective Field Theory (SMEFT) framework. In particular, it enables us to constrain anomalous electric dipole moments of the top quark, which are sensitive to physics beyond the SM [8–10]. On the other hand, $t\bar{t}j$ production at the LHC is key to study additional jet activity in $pp \to t\bar{t} + X$ events, since about half of these events are produced in association with extra jets [11–15]. In addition, it has been shown that, through $t\bar{t}j$ production, it is possible to extract the top-quark mass (m_t), as the normalized kinematic distribution constructed from the inverse $t\bar{t}j$ invariant mass is highly sensitive to m_t variations [16–18]. Furthermore, both $t\bar{t}j$ and $t\bar{t}\gamma$ production processes are also instrumental for investigating the top-quark charge asymmetry [19], and they serve as important SM backgrounds in many searches for new physics at the LHC.

Theoretical predictions for $pp \to t\bar{t}j$ and $pp \to t\bar{t}\gamma$ processes are available up to next-to-leading order (NLO) accuracy, including both QCD and EW corrections [20–35]. With experimental measurements reaching unprecedented precision in current and upcoming LHC runs, theoretical predictions must be provided at least at NNLO in QCD in order to match the experimental precision. Achieving this level of accuracy for either the $t\bar{t}j$ or $t\bar{t}\gamma$ production is a highly non-trivial task due to the algebraic and analytic complexity arising in the computation of the two-loop $2 \to 3$ scattering amplitudes. Significant progress has recently been made in evaluating two-loop $2 \to 3$ QCD scattering amplitudes involving massless internal particles [36–50]. This progress has been made possible thanks to the introduction of finite-field methods [51, 52], which streamline computations by avoiding intermediate large expressions. These also include those arising from the reduction of Feynman integrals via integration-by-parts identities (IBPs) [53–55] into a minimal basis known as master integrals (MIs). In addition, the efficient computation of the MIs via the differential equations method

(DEs) [56–60] has been enabled by the use of the canonical form of DEs [61] and the construction of bases of functions consisting of the independent components of the ϵ-expanded MIs, commonly known in the literature as *pentagon functions* [62–64]. Building upon these developments, two-loop Feynman integral studies have been initiated for processes involving top quarks such as $t\bar{t}j$ [65–67], $t\bar{t}H$ [68] and $t\bar{t}W$ [69] productions, and numerical results for the two-loop amplitudes are now available for the leading colour $t\bar{t}j$ production in gluon fusion [70] and for the N_f part of the process $q\bar{q} \rightarrow t\bar{t}H$ [71]. Moreover, in order to obtain NNLO QCD predictions, it is necessary to subtract both ultraviolet (UV) and infrared (IR) singularities from the two-loop scattering amplitudes and extract the finite remainder. This subtraction procedure requires UV renormalisation counterterms and the knowledge of the universal IR singularities, along with one-loop amplitudes expanded up to $\mathcal{O}(\epsilon^2)$ in the dimensional regularisation parameter, ϵ. While several automated packages are available to perform a computation of one-loop amplitudes [72–76], they can only be used for calculating up to the finite part, $\mathcal{O}(\epsilon^0)$, and the inclusion of higher ϵ terms will still require a dedicated effort. In this context, the relevant one-loop amplitudes for $2 \rightarrow 3$ processes involving a top-quark pair in the final state have been computed up to $\mathcal{O}(\epsilon^2)$ for the production channels: $gg/q\bar{q} \rightarrow t\bar{t}g$ [77], $gg \rightarrow t\bar{t}H$ [78] and $u\bar{d} \rightarrow t\bar{t}W^+$ [79].

The canonical DEs for the MIs associated to the pentagon topologies contributing to the one-loop $t\bar{t}j$ amplitude, as well as to the $t\bar{t}\gamma$ one-loop amplitude, have been studied in ref. [77], where the MIs have been evaluated by means of the generalised series expansion method [80, 81], as implemented in DiffExp [82]. In this work, we take a further step by expressing the MIs in terms of pentagon functions. Expressing the amplitude in terms of pentagon functions provides a natural framework for performing the Laurent expansion in the dimensional regulator, which is essential for isolating UV and IR divergences and extracting the finite remainder analytically. Another benefit of using a pentagon-function basis is that it usually leads to a significant simplification of the final expressions. In order to perform numerical evaluations of the amplitudes, we construct DEs for the pentagon-function basis and solve them numerically via generalised power series expansions, utilizing the packages DiffExp and Line [83]. We compute analytically the rational coefficients multiplying the pentagon functions using finite-field reconstruction techniques, which have been employed in numerous one- and two-loop multi-scale amplitude calculations. These techniques allow us to handle the complexity of the expressions at intermediate steps of the computation by replacing symbolic operations with numerical ones. We apply this method by exploiting the FiniteFlow framework [52, 84]. Furthermore, we consider the top quark on-shell and work in the helicity-amplitude representation, which provides a framework to efficiently include the top-quark decay process while preserving the information on spin correlation.

This paper is organized as follows. In section 2, we describe the colour structure of the one-loop amplitudes entering the $t\bar{t}j$ and $t\bar{t}\gamma$ production computations, as well as the helicity-amplitude computation starting from Feynman-diagram input. In section 3, we discuss the construction of the pentagon-function basis, the derivation of DEs for this basis and their numerical evaluation. In section 4, we provide numerical benchmark results of colour and helicity summed one-loop squared matrix elements up to $\mathcal{O}(\epsilon^2)$ for all possible channels appearing in the $pp \rightarrow t\bar{t}j$ and $pp \rightarrow t\bar{t}\gamma$ scattering processes. Finally, we conclude in section 5 with a summary of the results presented.

2   Helicity amplitudes

We compute one-loop QCD helicity amplitudes for the following partonic scattering processes entering the $pp \to t\bar{t}j$ production

$$0 \to \bar{t}(p_1) + t(p_2) + g(p_3) + g(p_4) + g(p_5), \tag{1}$$
$$0 \to \bar{t}(p_1) + t(p_2) + \bar{q}(p_3) + q(p_4) + g(p_5), \tag{2}$$

and the $pp \to t\bar{t}\gamma$ production

$$0 \to \bar{t}(p_1) + t(p_2) + g(p_3) + g(p_4) + \gamma(p_5), \tag{3}$$
$$0 \to \bar{t}(p_1) + t(p_2) + \bar{q}(p_3) + q(p_4) + \gamma(p_5), \tag{4}$$

where q represents a generic massless quark species. Some representative Feynman diagrams contributing to these processes are depicted in fig. 1.

All the external momenta, p_i, which live in the 4-dimensional space-time, are taken to be outgoing

$$p_1 + p_2 + p_3 + p_4 + p_5 = 0, \tag{5}$$

and fulfil the following on-shell conditions

$$p_1^2 = p_2^2 = m_t^2 \qquad \text{and} \qquad p_3^2 = p_4^2 = p_5^2 = 0. \tag{6}$$

We choose the following six scalar products and one pseudo-scalar invariant to describe the kinematics of the processes in eqs. (1) to (4),

$$\vec{x} = \left(d_{12}, d_{23}, d_{34}, d_{45}, d_{15}, m_t^2\right), \tag{7}$$
$$\mathrm{tr}_5 = 4\mathrm{i}\,\varepsilon_{\mu\nu\rho\sigma} p_1^\mu p_2^\nu p_3^\rho p_4^\sigma, \tag{8}$$

where $d_{ij} = p_i \cdot p_j$ and $\varepsilon_{\mu\nu\rho\sigma}$ is the anti-symmetric Levi-Civita pseudo-tensor.

2.1 $t\bar{t}j$ partial amplitudes

The colour decomposition of the L-loop amplitude in terms of partial amplitudes for the $0 \to \bar{t}tggg$ scattering process is given by

$$\mathcal{M}^{(L)}\left(1_{\bar{t}}, 2_t, 3_g, 4_g, 5_g\right) = \sqrt{2}\, g_s^3 \left[(4\pi)^\epsilon e^{-\epsilon \gamma_E} \frac{\alpha_s}{4\pi}\right]^L \times$$
$$\left\{ \sum_{\sigma \in S_3} (t^{a_{\sigma(3)}} t^{a_{\sigma(4)}} t^{a_{\sigma(5)}})^{\bar{i}_1}_{i_2}\, \mathcal{A}^{(L)}_{g;1}\left(1_{\bar{t}}, 2_t, \sigma(3)_g, \sigma(4)_g, \sigma(5)_g\right) \right.$$
$$+ \sum_{\sigma \in S_3'} \delta^{a_{\sigma(3)} a_{\sigma(4)}} (t^{a_{\sigma(5)}})^{\bar{i}_1}_{i_2}\, \mathcal{A}^{(L)}_{g;2}\left(1_{\bar{t}}, 2_t, \sigma(3)_g, \sigma(4)_g, \sigma(5)_g\right)$$
$$\left. + \sum_{\sigma \in \tilde{S}_3} \delta^{\bar{i}_1}_{i_2} \mathrm{tr}\left(t^{a_{\sigma(3)}} t^{a_{\sigma(4)}} t^{a_{\sigma(5)}}\right) \mathcal{A}^{(L)}_{g;3}\left(1_{\bar{t}}, 2_t, \sigma(3)_g, \sigma(4)_g, \sigma(5)_g\right) \right\},$$
$$\tag{9}$$

where g_s is the strong coupling constant, t^a are the $SU(N_c)$ generators in the fundamental representation normalised according to $\mathrm{tr}(t^a t^b) = \delta^{ab}/2$, $S_3' = S_3/\mathbb{Z}_2$, $\tilde{S}_3 = S_3/\mathbb{Z}_3$ and $\alpha_s = g_s^2/(4\pi)$. The sets of permutations entering eq. (9) are

$$S_3 = \{(3,4,5), (3,5,4), (4,3,5), (4,5,3), (5,3,4), (5,4,3)\},$$
$$S_3' = \{(3,4,5), (3,5,4), (4,5,3)\},$$
$$\tilde{S}_3 = \{(3,4,5), (3,5,4)\}.$$

$$A_{g;2}^{(1),1}(1,2,3,4,5), A_{g;3}^{(1),1}(1,2,3,5,4)$$

$l : A_{g;1}^{(1),n_f}(1,2,3,4,5), A_{g;3}^{(1),n_f/N_c}(1,2,3,4,5)$

$t : A_{g;1}^{(1),n_h}(1,2,3,4,5), A_{g;3}^{(1),n_h/N_c}(1,2,3,4,5)$

(a) $0 \to \bar{t}tggg$

$A_{q;1}^{(1),N_c}(1,2,3,4,5), A_{q;1}^{(1),1/N_c}(1,2,3,4,5),$
$A_{q;2}^{(1),1/N_c}(1,2,3,4,5)$

$l : A_{q;1}^{(1),n_f}(1,2,3,4,5), A_{q;3}^{(1),n_f}(1,2,3,4,5),$
$A_{q;4}^{(1),n_f}(1,2,3,4,5)$

$t : A_{q;1}^{(1),n_h}(1,2,3,4,5), A_{q;3}^{(1),n_h}(1,2,3,4,5),$
$A_{q;4}^{(1),n_h}(1,2,3,4,5)$

(b) $0 \to \bar{t}t\bar{q}qg$

$B_{g;1}^{(1),N_c}(1,2,3,4,5), B_{g;2}^{(1),1}(1,2,3,4,5)$

$l : B_{g;1}^{(1),n_f}(1,2,3,4,5)$

$t : B_{g;1}^{(1),n_h}(1,2,3,4,5)$

$l : B_{g;1l}^{(1),1}(1,2,3,4,5), B_{g;2l}^{(1),1/N_c}(1,2,3,4,5)$

$t : B_{g;1t}^{(1),1}(1,2,3,4,5), B_{g;2t}^{(1),1/N_c}(1,2,3,4,5)$

(c) $0 \to \bar{t}tgg\gamma$

$B_{t;1}^{(1),N_c}(1,2,3,4,5), B_{t;1}^{(1),1/N_c}(1,2,3,4,5),$
$B_{t;2}^{(1),1/N_c}(1,2,3,4,5)$

$l : B_{q;1}^{(1),n_f}(1,2,3,4,5), B_{q;2}^{(1),n_f}(1,2,3,4,5)$

$t : B_{q;1}^{(1),n_h}(1,2,3,4,5), B_{q;2}^{(1),n_h}(1,2,3,4,5)$
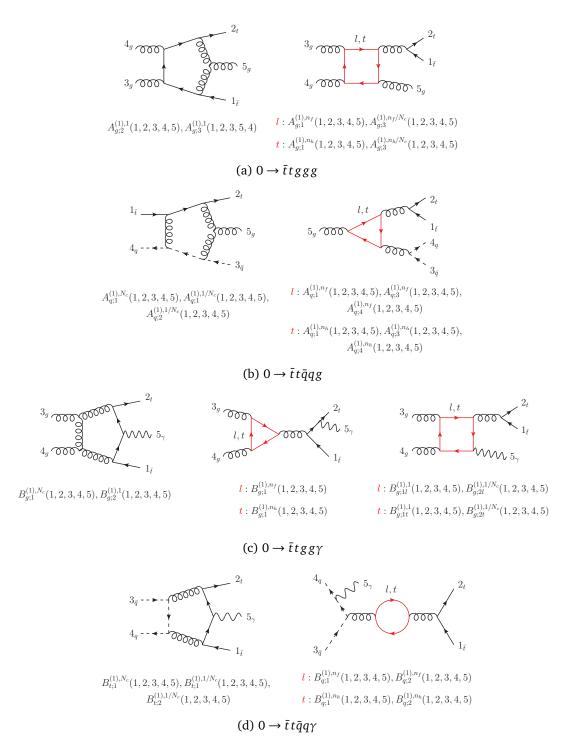
(d) $0 \to \bar{t}t\bar{q}q\gamma$

Figure 1: Sample Feynman diagrams contributing to one-loop $pp \to t\bar{t}j$ and $pp \to t\bar{t}\gamma$ amplitudes, together with the partial amplitudes that they contribute to. Black solid (dashed) lines represent top (massless) quarks associated with open fermion lines. Moreover, wavy lines denote photons, and curly lines denote gluons. Either massless quark ($l \in \{u,d,c,s,b\}$), or top-quark (t) can circulate in the red closed fermion loop, giving rise to n_l-, n_h-, $1l/2l$- and $1t/2t$-type partial amplitudes.

Each partial amplitude, $\mathcal{A}_{g;i}^{(L)}$, can further be decomposed according to their dependence on N_c as well as the number of massless (n_f) and massive (n_h) closed fermion loops. At one-loop

level, this decomposition reads

$$\mathcal{A}_{g;1}^{(1)} = N_c A_{g;1}^{(1),N_c} + \frac{1}{N_c} A_{g;1}^{(1),1/N_c} + n_f A_{g;1}^{(1),n_f} + n_h A_{g;1}^{(1),n_h}, \tag{10a}$$

$$\mathcal{A}_{g;2}^{(1)} = A_{g;2}^{(1),1}, \tag{10b}$$

$$\mathcal{A}_{g;3}^{(1)} = A_{g;3}^{(1),1} + \frac{n_f}{N_c} A_{g;3}^{(1),n_f/N_c} + \frac{n_h}{N_c} A_{g;3}^{(1),n_h/N_c}. \tag{10c}$$

In the case of $0 \to \bar{t}t\bar{q}qg$ process, the L-loop colour decomposition is given by

$$\mathcal{M}^{(L)}\big(1_{\bar{t}}, 2_t, 3_{\bar{q}}, 4_q, 5_g\big) = \sqrt{2}\, g_s^3 \left[(4\pi)^\epsilon e^{-\epsilon\gamma_E} \frac{\alpha_s}{4\pi} \right]^L \times$$

$$\left\{ \delta_{i_4}^{\bar{i}_1} (t^{a_5})_{i_2}^{\bar{i}_3} \, \mathcal{A}_{q;1}^{(L)}\big(1_{\bar{t}}, 2_t, 3_{\bar{q}}, 4_q, 5_g\big) \right.$$

$$+ \delta_{i_2}^{\bar{i}_3} (t^{a_5})_{i_4}^{\bar{i}_1} \, \mathcal{A}_{q;2}^{(L)}\big(1_{\bar{t}}, 2_t, 3_{\bar{q}}, 4_q, 5_g\big) \tag{11}$$

$$+ \frac{1}{N_c} \delta_{i_2}^{\bar{i}_1} (t^{a_5})_{i_4}^{\bar{i}_3} \, \mathcal{A}_{q;3}^{(L)}\big(1_{\bar{t}}, 2_t, 3_{\bar{q}}, 4_q, 5_g\big)$$

$$\left. + \frac{1}{N_c} \delta_{i_4}^{\bar{i}_3} (t^{a_5})_{i_2}^{\bar{i}_1} \, \mathcal{A}_{q;4}^{(L)}\big(1_{\bar{t}}, 2_t, 3_{\bar{q}}, 4_q, 5_g\big) \right\},$$

and the one-loop partial amplitude decomposition in terms of N_c, n_f and n_h reads

$$\mathcal{A}_{q;z}^{(1)} = N_c A_{q;z}^{(1),N_c} + \frac{1}{N_c} A_{q;z}^{(1),1/N_c} + n_f A_{q;z}^{(1),n_f} + n_h A_{q;z}^{(1),n_h}, \tag{12}$$

where $z \in \{1, \dots, 4\}$.

We derive analytic expressions for the gauge invariant mass-renormalised amplitude

$$\mathcal{A}_{\mathrm{mren}}^{(1)} = \mathcal{A}^{(1)} + \delta Z_m^{(1)} \mathcal{A}_{\mathrm{mct}}^{(0)}, \tag{13}$$

which is obtained by adding the tree-level amplitude with the one-loop mass counterterm insertion ($\mathcal{A}_{\mathrm{mct}}^{(0)}$) to the bare amplitude ($\mathcal{A}^{(1)}$). Furthermore, $\delta Z_m^{(1)}$ is denoting the one-loop top-quark mass-renormalisation constant. The fully UV-renormalised amplitude is obtained by including the counterterms associated with the strong coupling constant, as well as the renormalisation of the top-quark and gluon external wavefunctions,

$$\mathcal{A}_{\mathrm{ren}}^{(1)} = \mathcal{A}_{\mathrm{mren}}^{(1)} + \left(\delta Z_t^{(1)} + \frac{3}{2} \delta Z_{\alpha_s}^{(1)} + \frac{n_g}{2} \delta Z_g^{(1)} \right) \mathcal{A}^{(0)}, \tag{14}$$

where n_g is the number of external gluons involved in the scattering process ($n_g = 3$ for $0 \to \bar{t}tggg$ and $n_g = 1$ for $0 \to \bar{t}t\bar{q}qg$). The expressions of the one-loop renormalisation constants $\delta Z_m^{(1)}$, $\delta Z_t^{(1)}$ and $\delta Z_{\alpha_s}^{(1)}$ are provided in the appendix A.

2.2 $t\bar{t}\gamma$ partial amplitudes

We now turn to the colour decomposition of the L-loop amplitudes contributing to the production of $t\bar{t}\gamma$ final state in pp collisions. For the gluon channel, $0 \to \bar{t}tgg\gamma$, the decomposition

is given by

$$\mathcal{M}^{(L)}\left(1_{\bar{t}}, 2_t, 3_g, 4_g, 5_\gamma\right) = \sqrt{2}\, e\, g_s^2 \left[(4\pi)^\epsilon e^{-\epsilon \gamma_E} \frac{\alpha_s}{4\pi}\right]^L \times$$

$$\left\{ (t^{a_3} t^{a_4})_{i_2}^{\bar{i}_1}\, \mathcal{B}_{g;1}^{(L)}\left(1_{\bar{t}}, 2_t, 3_g, 4_g, 5_\gamma\right) \right.$$

$$+ (t^{a_4} t^{a_3})_{i_2}^{\bar{i}_1}\, \mathcal{B}_{g;1}^{(L)}\left(1_{\bar{t}}, 2_t, 4_g, 3_g, 5_\gamma\right) \tag{15}$$

$$\left. + \delta_{i_2}^{\bar{i}_1} \delta^{a_3 a_4}\, \mathcal{B}_{g;2}^{(L)}\left(1_{\bar{t}}, 2_t, 3_g, 4_g, 5_\gamma\right) \right\},$$

where e is the magnitude of the electron charge. Similarly to the $t\bar{t}j$ amplitudes, the $t\bar{t}\gamma$ one-loop partial amplitudes, $\mathcal{B}_{g;i}^{(L)}$, are further decomposed into sub-amplitudes according to the different types of closed fermion loops present:

$$\mathcal{B}_{g;1}^{(1)} = Q_t N_c B_{g;1}^{(1),N_c} + \frac{Q_t}{N_c} B_{g;1}^{(1),1/N_c} + Q_t n_f B_{g;1}^{(1),n_f} + Q_t n_h B_{g;1}^{(1),n_h} + \tilde{Q}_l B_{g;1l}^{(1),1} + Q_t B_{g;1t}^{(1),1}, \tag{16a}$$

$$\mathcal{B}_{g;2}^{(1)} = B_{g;2}^{(1),1} + \tilde{Q}_l B_{g;2l}^{(1),1/N_c} + Q_t B_{g;2t}^{(1),1/N_c}. \tag{16b}$$

In the expressions above, $\tilde{Q}_l = \sum_l Q_l$, with Q_t and Q_l being the fractional charges of the top quark and of the massless quark ($l \in \{u, d, c, s, b\}$), respectively. In addition to the n_f- and n_h-type amplitudes, the $0 \to \bar{t}tgg\gamma$ colour decomposition contains contributions from diagrams where the photon couples to the internal quark closed-loop instead of the top-quark line ($B_{g;1l}^{(1),1}, B_{g;1t}^{(1),1}, B_{g;2l}^{(1),1/N_c}, B_{g;2t}^{(1),1/N_c}$), as shown in the rightmost Feynman diagram in fig. 1c.

For the $0 \to \bar{t}t\bar{q}q\gamma$ scattering amplitude, the L-loop colour decomposition is

$$\mathcal{M}^{(L)}\left(1_{\bar{t}}, 2_t, 3_{\bar{q}}, 4_q, 5_\gamma\right) = \sqrt{2}\, e\, g_s^2 \left[(4\pi)^\epsilon e^{-\epsilon \gamma_E} \frac{\alpha_s}{4\pi}\right]^L \times$$

$$\left\{ \delta_{i_4}^{\bar{i}_1} \delta_{i_2}^{\bar{i}_3} \left[Q_t\, \mathcal{B}_{t;1}^{(L)}\left(1_{\bar{t}}, 2_t, 3_{\bar{q}}, 4_q, 5_\gamma\right) + Q_q\, \mathcal{B}_{q;1}^{(L)}\left(1_{\bar{t}}, 2_t, 3_{\bar{q}}, 4_q, 5_\gamma\right) \right] \right.$$

$$\left. + \frac{1}{N_c} \delta_{i_2}^{\bar{i}_1} \delta_{i_4}^{\bar{i}_3} \left[Q_t\, \mathcal{B}_{t;2}^{(L)}\left(1_{\bar{t}}, 2_t, 3_{\bar{q}}, 4_q, 5_\gamma\right) + Q_q\, \mathcal{B}_{q;2}^{(L)}\left(1_{\bar{t}}, 2_t, 3_{\bar{q}}, 4_q, 5_\gamma\right) \right] \right\}. \tag{17}$$

In this case, the photon can be coupled either to the top quark or to the massless quark q, such that the corresponding partial amplitude picks up either Q_t or the fractional charge of the massless quark Q_q. Equivalently to the $0 \to \bar{t}t\bar{q}qg$ case, the one-loop $0 \to \bar{t}t\bar{q}q\gamma$ partial amplitudes can be decomposed into sub-amplitude according to the N_c, n_f and n_h contribution,

$$\mathcal{B}_{z;i}^{(1)} = N_c B_{z;i}^{(1),N_c} + \frac{1}{N_c} B_{z;i}^{(1),1/N_c} + n_f B_{z;i}^{(1),n_f} + n_h B_{z;i}^{(1),n_h}, \tag{18}$$

where $z \in \{t, q\}$ and $i \in \{1, 2\}$. We note that in $0 \to \bar{t}t\bar{q}q\gamma$ process, partial amplitudes where the photon is coupled to the internal quark loop do not appear due to Furry's theorem.

The mass-renormalised amplitude, which is gauge invariant, is given by

$$\mathcal{B}_{\mathrm{mren}}^{(1)} = \mathcal{B}^{(1)} + \delta Z_m^{(1)} \mathcal{B}_{\mathrm{mct}}^{(0)}, \tag{19}$$

while the fully renormalised $t\bar{t}\gamma$ amplitude is constructed by including the appropriate UV counterterms,

$$\mathcal{B}_{\mathrm{ren}}^{(1)} = \mathcal{B}_{\mathrm{mren}}^{(1)} + \left(\delta Z_t^{(1)} + \delta Z_{\alpha_s}^{(1)} + n_g \delta Z_g^{(1)}\right) \mathcal{B}^{(0)}. \tag{20}$$

Here, we have $n_g = 2$ for $0 \to \bar{t}tgg\gamma$, and $n_g = 0$ for $0 \to \bar{t}t\bar{q}q\gamma$.

2.3 Helicity-amplitude computation

Our construction of helicity amplitudes for $pp \to t\bar{t}j$ and $pp \to t\bar{t}\gamma$ productions in the t Hooft-Veltman scheme (tHV) starts with the decomposition of the partial amplitudes in terms of independent 4-dimensional tensor structures [85, 86]

$$
A_{\text{g}}^{(L)} = \sum_{i=1}^{32} \mathcal{T}_{\text{g},i}\, \mathcal{F}_{\text{g},i}^{(L)}\,,
$$
$$
A_{\text{q}}^{(L)} = \sum_{i=1}^{16} \mathcal{T}_{\text{q},i}\, \mathcal{F}_{\text{q},i}^{(L)}\,,
$$
(21)

where $A_{\text{g}}^{(L)}$ represents either $0 \to \bar{t}tggg$ or $0 \to \bar{t}tgg\gamma$ amplitudes, while $A_{\text{q}}^{(L)}$ stands for either $0 \to \bar{t}t\bar{q}qg$ or $0 \to \bar{t}t\bar{q}q\gamma$ amplitudes. The tensor structures for the $0 \to \bar{t}tggg$ and $0 \to \bar{t}tgg\gamma$ amplitudes are

$$
\begin{aligned}
\mathcal{T}_{\text{g},1\dots8} &= m_t^2\, \bar{u}(p_2) v(p_1)\, \Gamma_{\text{g},1\dots8}\,, \\
\mathcal{T}_{\text{g},9\dots16} &= m_t\, \bar{u}(p_2) \slashed{p}_3 v(p_1)\, \Gamma_{\text{g},1\dots8}\,, \\
\mathcal{T}_{\text{g},17\dots24} &= m_t\, \bar{u}(p_2) \slashed{p}_4 v(p_1)\, \Gamma_{\text{g},1\dots8}\,, \\
\mathcal{T}_{\text{g},25\dots32} &= \bar{u}(p_2) \slashed{p}_3 \slashed{p}_4 v(p_1)\, \Gamma_{\text{g},1\dots8}\,,
\end{aligned}
$$
(22)

while for the $0 \to \bar{t}t\bar{q}qg$ or $0 \to \bar{t}t\bar{q}q\gamma$ amplitudes they are

$$
\begin{aligned}
\mathcal{T}_{\text{q},1\dots4} &= m_t^2\, \bar{u}(p_2) v(p_1)\, \Gamma_{\text{q},1\dots4}\,, \\
\mathcal{T}_{\text{q},5\dots8} &= m_t\, \bar{u}(p_2) \slashed{p}_3 v(p_1)\, \Gamma_{\text{q},1\dots4}\,, \\
\mathcal{T}_{\text{q},9\dots12} &= m_t\, \bar{u}(p_2) \slashed{p}_4 v(p_1)\, \Gamma_{\text{q},1\dots4}\,, \\
\mathcal{T}_{\text{q},13\dots16} &= \bar{u}(p_2) \slashed{p}_3 \slashed{p}_4 v(p_1)\, \Gamma_{\text{q},1\dots4}\,.
\end{aligned}
$$
(23)

In eqs. (22) and (23) we have separated the top-quark spinor strings from the tensor structures of the massless particles. The tensor structures involving three massless vector bosons are given by

$$
\begin{aligned}
\Gamma_{\text{g},1} &= p_1 \cdot \varepsilon(p_3)\, p_1 \cdot \varepsilon(p_4)\, p_1 \cdot \varepsilon(p_5)\,, \\
\Gamma_{\text{g},2} &= p_1 \cdot \varepsilon(p_3)\, p_1 \cdot \varepsilon(p_4)\, p_2 \cdot \varepsilon(p_5)\,, \\
\Gamma_{\text{g},3} &= p_1 \cdot \varepsilon(p_3)\, p_2 \cdot \varepsilon(p_4)\, p_1 \cdot \varepsilon(p_5)\,, \\
\Gamma_{\text{g},4} &= p_2 \cdot \varepsilon(p_3)\, p_1 \cdot \varepsilon(p_4)\, p_1 \cdot \varepsilon(p_5)\,, \\
\Gamma_{\text{g},5} &= p_1 \cdot \varepsilon(p_3)\, p_2 \cdot \varepsilon(p_4)\, p_2 \cdot \varepsilon(p_5)\,, \\
\Gamma_{\text{g},6} &= p_2 \cdot \varepsilon(p_3)\, p_1 \cdot \varepsilon(p_4)\, p_2 \cdot \varepsilon(p_5)\,, \\
\Gamma_{\text{g},7} &= p_2 \cdot \varepsilon(p_3)\, p_2 \cdot \varepsilon(p_4)\, p_1 \cdot \varepsilon(p_5)\,, \\
\Gamma_{\text{g},8} &= p_2 \cdot \varepsilon(p_3)\, p_2 \cdot \varepsilon(p_4)\, p_2 \cdot \varepsilon(p_5)\,,
\end{aligned}
$$
(24)

while those involving a massless quark pair and a massless vector boson are

$$
\begin{aligned}
\Gamma_{\text{q},1} &= \bar{u}(p_4) \slashed{p}_1 v(p_3)\, p_1 \cdot \varepsilon(p_5)\,, \\
\Gamma_{\text{q},2} &= \bar{u}(p_4) \slashed{p}_1 v(p_3)\, p_2 \cdot \varepsilon(p_5)\,, \\
\Gamma_{\text{q},3} &= \bar{u}(p_4) \slashed{p}_2 v(p_3)\, p_1 \cdot \varepsilon(p_5)\,, \\
\Gamma_{\text{q},4} &= \bar{u}(p_4) \slashed{p}_2 v(p_3)\, p_2 \cdot \varepsilon(p_5)\,.
\end{aligned}
$$
(25)

In writing $\Gamma_{\text{g},i}$ and $\Gamma_{\text{q},i}$, $\varepsilon(p_i) \cdot p_i = 0$ and $\varepsilon(p_i) \cdot q_i = 0$ (where q_i is the reference momentum associated with the polarisation vector $\varepsilon(p_i)$) have been enforced and we have chosen $q_3 = p_4$,

$q_4 = p_3$ and $q_5 = p_3$. This set of reference vectors is chosen arbitrarily, however, different choice of such vectors will lead to different set of tensor structures. The form factor, $\mathcal{F}_{\text{g/q};i}^{(L)}$, is obtained by multiplying the partial amplitudes in eq. (21) with the conjugated tensor structure $\mathcal{T}_{\text{g/q};i}^{\dagger}$, summing over the polarisations of the external states, and inverting the resulting linear system of equations, so that

$$\mathcal{F}_{\text{g/q};i}^{(L)} = \sum_{j=1}^{n_{\mathcal{T}}} \left(\Delta_{\text{g/q}}^{-1} \right)_{ij} \tilde{A}_{\text{g/q};j}^{(L)}, \tag{26}$$

where we have defined the so-called *contracted partial amplitude*

$$\tilde{A}_{\text{g/q};i}^{(L)} = \sum_{\text{pol}} T_{\text{g/q};i}^{\dagger} A_{\text{g/q}}^{(L)}, \tag{27}$$

while the linear system to be inverted is defined through the matrix

$$\Delta_{\text{g/q};ij} = \sum_{\text{pol}} \mathcal{T}_{\text{g/q};i}^{\dagger} \mathcal{T}_{\text{g/q};j}. \tag{28}$$

In eq. (26), $n_{\mathcal{T}}$ is the number of tensor structures appearing in eqs. (22) and (23), i.e. $n_{\mathcal{T}}(\text{g}) = 32$ and $n_{\mathcal{T}}(\text{q}) = 16$. We employ the following polarisation sum for the massless vector boson,

$$\sum_{\text{pol}} \varepsilon_{\mu}^*(p_i, q_i) \varepsilon_{\nu}(p_i, q_i) = -g_{\mu\nu} + \frac{p_{i\mu} q_{i\nu} + q_{i\mu} p_{i\nu}}{p_i \cdot q_i}, \tag{29}$$

with q_i being the massless reference momentum for the external polarisation vector.

The helicity amplitude is then obtained by specifying the helicity/spin states of the spinors and polarisation vectors in the tensor structures in eqs. (22) to (25). We follow the approach of ref. [87] to specify the spin states of the massive spinors, where the massive spinor is defined starting from the massless helicity spinor with the introduction of an arbitrary reference direction n^{μ}

$$\bar{u}_+(p_2, m_t) = \frac{\langle n_2 |(\not{p}_2 + m_t)}{\langle n_2 p_2^{\flat} \rangle}, \qquad v_+(p_1, m_t) = \frac{(\not{p}_1 - m_t)|n_1\rangle}{\langle p_1^{\flat} n_1 \rangle}, \tag{30}$$

where we have used the following decomposition for the top quark and anti-top quark momenta (p_1 and p_2, respectively),

$$p_i^{\mu} = p_i^{\flat,\mu} + \frac{m_t^2}{p_i^{\flat} \cdot n_i} n_i^{\mu}, \tag{31}$$

with $n_i^2 = 0$, $(p_i^{\flat})^2 = 0$ and $i = 1, 2$. Having this massive spinor prescription, we can express the helicity amplitude in terms of massless momenta ($p_1^{\flat}, p_2^{\flat}, p_3, p_4, p_5$) in the basis of reference vectors n_1 and n_2 as follows [77, 88],

$$
\begin{aligned}
A^{(L)}(1_{\bar{t}}^+, 2_t^+, 3^{h_3}, 4^{h_4}, 5^{h_5}; n_1, n_2) = \frac{m_t \, \Phi^{h_3 h_4 h_5}}{\langle 1^{\flat} n_1 \rangle \langle 2^{\flat} n_2 \rangle} &\Big\{ \langle n_1 n_2 \rangle s_{34} A^{(L),[1]}(1_{\bar{t}}^+, 2_t^+, 3^{h_3}, 4^{h_4}, 5^{h_5}) \\
&+ \langle n_1 3 \rangle \langle n_2 4 \rangle [34] A^{(L),[2]}(1_{\bar{t}}^+, 2_t^+, 3^{h_3}, 4^{h_4}, 5^{h_5}) \\
&+ \langle n_1 3 \rangle \langle n_2 3 \rangle \frac{[3|4|5|3]}{s_{34}} A^{(L),[3]}(1_{\bar{t}}^+, 2_t^+, 3^{h_3}, 4^{h_4}, 5^{h_5}) \\
&+ \langle n_1 4 \rangle \langle n_2 4 \rangle \frac{[4|5|3|4]}{s_{34}} A^{(L),[4]}(1_{\bar{t}}^+, 2_t^+, 3^{h_3}, 4^{h_4}, 5^{h_5}) \Big\}.
\end{aligned}
\tag{32}
$$

We only write down the "+" configuration for the massive spinor since the corresponding "-" configuration can be obtained by swapping the momenta $n \leftrightarrow p^\flat$ in eq. (30). In eq. (32), the phase factors Φ depend on the helicity configuration of the massless particles. They are chosen in such a way that the sub-amplitudes $A^{(L),[i]}$ are free of spinor phase and dimensionless. For the $0 \to \bar{t}tggg$ and $0 \to \bar{t}tgg\gamma$ scattering processes, the phase factors Φ are

$$\Phi^{+++} = \frac{[35]}{s_{34}\langle 34\rangle\langle 45\rangle}\,, \tag{33a}$$

$$\Phi^{++-} = \frac{\langle 5|3|4|5\rangle}{s_{34}^2\langle 34\rangle^2}\,, \tag{33b}$$

$$\Phi^{+-+} = \frac{\langle 4|5|3|4\rangle}{s_{34}^2\langle 35\rangle^2}\,, \tag{33c}$$

$$\Phi^{-++} = \frac{\langle 3|5|4|3\rangle}{s_{34}^2\langle 45\rangle^2}\,, \tag{33d}$$

while for the $0 \to \bar{t}t\bar{q}qg$ and $0 \to \bar{t}t\bar{q}q\gamma$, they are given by

$$\Phi^{+-+} = \frac{\langle 34\rangle[35]}{s_{34}^2\langle 35\rangle}\,, \tag{34a}$$

$$\Phi^{-++} = \frac{\langle 34\rangle[45]}{s_{34}^2\langle 45\rangle}\,. \tag{34b}$$

We computed the following helicity configurations for the massless particles: for the $0 \to \bar{t}tggg$ and $0 \to \bar{t}tgg\gamma$ processes, we considered the $+++$, $++-$, $+-+$, and $-++$ configurations. For the $0 \to \bar{t}t\bar{q}qg$ and $0 \to \bar{t}t\bar{q}q\gamma$ processes, we only considered the $+-+$ and $-++$ configurations. The remaining helicity configurations can be obtained by performing parity conjugation on the existing helicity amplitudes. We emphasize that our treatment of external massive spinor is not unique, and different representations can be employed [89], including the ones where a specific massive spinor description in not required, but instead using a form factor decomposotion only for massive spinor strings [78].

To derive the helicity sub-amplitudes ($A^{(L),[i]}$ in eq. (32)), we first evaluate the helicity amplitude in eq. (32) at four different choices of reference vectors

$$\mathfrak{A}^{(L),h_3h_4h_5} = \begin{pmatrix} A^{(L)}(1_{\bar{t}}^+, 2_t^+, 3^{h_3}, 4^{h_4}, 5^{h_5}; p_3, p_3) \\ A^{(L)}(1_{\bar{t}}^+, 2_t^+, 3^{h_3}, 4^{h_4}, 5^{h_5}; p_3, p_4) \\ A^{(L)}(1_{\bar{t}}^+, 2_t^+, 3^{h_3}, 4^{h_4}, 5^{h_5}; p_4, p_3) \\ A^{(L)}(1_{\bar{t}}^+, 2_t^+, 3^{h_3}, 4^{h_4}, 5^{h_5}; p_4, p_4) \end{pmatrix}\,, \tag{35}$$

which we will refer to as *projected helicity amplitudes* in the following. By inserting the four choices of n_1 and n_2 in eq. (32) and inverting the resulting system of equations, the helicity sub-amplitudes can be written in terms of projected helicity amplitude $\mathfrak{A}^{(L),h_3h_4h_5}$ elements as

$$A^{(L),[i]}(1_{\bar{t}}^+, 2_t^+, 3^{h_3}, 4^{h_4}, 5^{h_5}) = \sum_{j=1}^{4} \alpha_{ij}^{h_3h_4h_5} \mathfrak{A}_j^{(L),h_3h_4h_5}\,, \tag{36}$$

where the non-zero entries of $\alpha_{ij}^{h_3 h_4 h_5}$ are

$$
\alpha_{12}^{h_3 h_4 h_5} = \alpha_{22}^{h_3 h_4 h_5} = \frac{1}{m_t \Phi^{h_3 h_4 h_5}} \frac{\langle 1^\flat 3 \rangle \langle 2^\flat 4 \rangle}{s_{34} \langle 34 \rangle} \bigg|_{n_1 = p_3, n_2 = p_4},
$$

$$
\alpha_{23}^{h_3 h_4 h_5} = \frac{1}{m_t \Phi^{h_3 h_4 h_5}} \frac{\langle 1^\flat 4 \rangle \langle 2^\flat 3 \rangle}{s_{34} \langle 34 \rangle} \bigg|_{n_1 = p_4, n_2 = p_3},
$$

$$
\alpha_{34}^{h_3 h_4 h_5} = -\frac{1}{m_t \Phi^{h_3 h_4 h_5}} \frac{\langle 1^\flat 4 \rangle \langle 2^\flat 4 \rangle}{\langle 4|5|3|4 \rangle} \bigg|_{n_1 = p_4, n_2 = p_4},
$$

$$
\alpha_{41}^{h_3 h_4 h_5} = -\frac{1}{m_t \Phi^{h_3 h_4 h_5}} \frac{\langle 1^\flat 3 \rangle \langle 2^\flat 3 \rangle}{\langle 3|4|5|3 \rangle} \bigg|_{n_1 = p_3, n_2 = p_3}.
$$

$$(37)$$

The projected helicity amplitudes $\mathfrak{A}^{(L), h_3 h_4 h_5}$ are obtained from the contracted partial amplitudes, $\tilde{A}_{g/q;i}^{(L)}$ in eq. (27), through

$$
\mathfrak{A}_i^{(L), h_3 h_4 h_5} = \sum_{j,k=1}^{n_\mathcal{T}} \Theta_{g/q;ij}^{h_3 h_4 h_5} \left(\Delta_{g/q}^{-1} \right)_{jk} \tilde{A}_{g/q;k}^{(L)}. \tag{38}
$$

The helicity-dependent matrix Θ is built out of tensor structures in eqs. (22) and (23), where the spin/helicity states have been chosen such that

$$
\mathcal{T}_{g/q;i} \rightarrow \mathcal{T}_{g/q;i}^{++h_3 h_4 h_5}(n_1, n_2), \tag{39}
$$

with the reference vectors (n_1, n_2) evaluated at four different values as in eq. (35),

$$
\Theta_{g/q}^{h_3 h_4 h_5} = \begin{pmatrix}
\mathcal{T}_{g/q;1}^{++h_3 h_4 h_5}(p_3, p_3) & \cdots & \mathcal{T}_{g/q;n_\mathcal{T}}^{++h_3 h_4 h_5}(p_3, p_3) \\
\mathcal{T}_{g/q;1}^{++h_3 h_4 h_5}(p_3, p_4) & \cdots & \mathcal{T}_{g/q;n_\mathcal{T}}^{++h_3 h_4 h_5}(p_3, p_4) \\
\mathcal{T}_{g/q;1}^{++h_3 h_4 h_5}(p_4, p_3) & \cdots & \mathcal{T}_{g/q;n_\mathcal{T}}^{++h_3 h_4 h_5}(p_4, p_3) \\
\mathcal{T}_{g/q;1}^{++h_3 h_4 h_5}(p_4, p_4) & \cdots & \mathcal{T}_{g/q;n_\mathcal{T}}^{++h_3 h_4 h_5}(p_4, p_4)
\end{pmatrix}. \tag{40}
$$

Finally, the helicity sub-amplitudes are derived from the contracted partial amplitudes $\tilde{A}_{g/q;i}^{(L)}$ as follows

$$
A^{(L),[i]}(1_{\bar{t}}^+, 2_t^+, 3^{h_3}, 4^{h_4}, 5^{h_5}) = \sum_{j=1}^{4} \sum_{k,l=1}^{n_\mathcal{T}} \alpha_{ij}^{h_3 h_4 h_5} \Theta_{g/q;jk}^{h_3 h_4 h_5} \left(\Delta_{g/q}^{-1} \right)_{kl} \tilde{A}_{g/q;l}^{(L)}. \tag{41}
$$

Equipped with a prescription to construct helicity amplitudes for $pp \rightarrow t\bar{t}j$ and $pp \rightarrow t\bar{t}\gamma$, we now turn the discussion to the analytic computation framework. Our amplitude calculations follow the Feynman diagrammatic method, combined with finite-field arithmetic [51,52], which has been successfully used for the analytic computation of various two-loop five-point amplitudes (e.g., [37, 42, 49]). The calculation begins with the generation of Feynman diagrams using QGRAF [90], followed by the colour decomposition in order to extract partial amplitudes according to the structures discussed in section 2.1. For each partial amplitude, we construct the one-loop contracted partial amplitude $\tilde{A}_{g/q;i}^{(1)}$ using in-house scripts which utilise MATHEMATICA and FORM [91]. The one-loop contracted partial amplitudes are expressed as a linear combination of scalar Feynman integrals, which are further reduced onto the set of MIs introduced in ref. [77] by means of IBP reduction [53–55]. We make use of NEATIBP package [92] to generate an optimized system of IBP identities. The contracted partial amplitudes, as well as the MIs, are then Laurent-expanded around $\epsilon = 0$, keeping terms up to order ϵ^2.

The components of the MIs in this expansion are written, order by order in ϵ, as polynomials in the pentagon-function basis, the construction of which is discussed in detail in section 3.

The series of algebraic operations discussed so far are executed numerically over finite fields using the FINITEFLOW package [52, 84], starting with the contracted partial amplitude $\tilde{A}^{(1)}_{g/q;i}$, proceeding through the solution of the IBP identities, and ending with the determination of the one-loop helicity sub-amplitudes $A^{(1),[i]}$ as given in eq. (41). This framework allows us to evaluate numerically over finite fields the rational coefficients of the pentagon functions appearing in the helicity sub-amplitudes, which we exploit to reconstruct the corresponding analytic expressions. We employ several techniques to reduce the complexity of the analytical reconstruction, such as finding linear relations among rational coefficients, guessing the denominator of the rational coefficients and on-the-fly univariate partial fraction decomposition. For further details on the analytic reconstruction strategies that we used, see refs. [42, 44]. In addition, performing evaluations over finite fields requires a rational parametrisation of the external kinematics, for which we employ the momentum-twistor parametrisation [88, 93, 94] of ref. [77]. With this parametrisation, spinor products and Mandelstam invariants entering the $\alpha^{h_3 h_4 h_5}$, $\Theta^{h_3 h_4 h_5}_{g/q}$ and $\Delta_{g/q}$ matrices together with the contracted partial amplitude $\tilde{A}^{(L)}_{g/q}$ in eq. (41) can be written as rational functions in the momentum-twistor variables $\vec{t} = (s_{34}, t_{12}, t_{23}, t_{45}, t_{15}, x_{1523})$ [1].

The resulting analytic expressions for the mass-renormalised one-loop $pp \to t\bar{t}j$ and $pp \to t\bar{t}\gamma$ helicity sub-amplitudes are further post-processed to extract the finite remainders, which are obtained including the UV and infrared (IR) counterterms according to

$$
\begin{aligned}
F^{(L),[i]}(1^+_{\bar{t}}, 2^+_t, 3^{h_3}, 4^{h_4}, 5^{h_5}) = {} & A^{(L),[i]}_{\mathrm{mren}}(1^+_{\bar{t}}, 2^+_t, 3^{h_3}, 4^{h_4}, 5^{h_5}) + A^{(L),[i]}_{\mathrm{UV}}(1^+_{\bar{t}}, 2^+_t, 3^{h_3}, 4^{h_4}, 5^{h_5}) \\
& - A^{(L),[i]}_{\mathrm{IR}}(1^+_{\bar{t}}, 2^+_t, 3^{h_3}, 4^{h_4}, 5^{h_5}).
\end{aligned}
\tag{42}
$$

The UV counterterms are given in eqs. (14) and (20) for the $t\bar{t}j$ and $t\bar{t}\gamma$ processes, respectively. The IR counterterms are known from the universal factorisation of the QCD amplitudes [95–100]. For the $t\bar{t}j$ process the IR counterterms have been computed explicitly in [77] while for the $t\bar{t}\gamma$ amplitude, the IR pole formula can be obtained from that of $pp \to t\bar{t}$ production [101]. In extracting the finite remainder we have adopted the $\overline{\mathrm{MS}}$ scheme [97], where at one-loop level the finite remainder is essentially the UV renormalised amplitude with the $1/\epsilon^2$ and $1/\epsilon$ poles removed. We stress that the analytic extraction of the finite remainder is made possible thanks to the expansion of master integrals in terms of pentagon function basis. Analytic form of the finite remainder, UV and IR counterterms for each helicity subamplitudes are provided in the ancillary files accompanying this article [102] under the anc/amplitudes/ directory.

Before closing this section, we would like to briefly discuss some observations on the algebraic complexity of the rational coefficients appearing in the one-loop $t\bar{t}j$ and $t\bar{t}\gamma$ amplitudes through $\mathcal{O}(\epsilon^2)$. In table 1 we show the highest numerator degree of the rational coefficients of the pentagon functions for the most complicated leading and subleading colour contributions in $0 \to \bar{t}tggg$ and $0 \to \bar{t}tgg\gamma$ processes. We note that the denominators in the rational coefficients of the pentagon functions are fully known by matching them to the letters corresponding to the master integrals. For both processes, we clearly observe an increase in the degrees going from leading- to subleading-colour terms. Multiple stages of optimisation in our analytic reconstruction framework, particularly that of univariate partial fraction decomposition, have proven to be highly effective in reducing the algebraic complexity of the expressions to be reconstructed. In this work, we further perform multivariate partial fraction decomposition on the reconstructed analytic expressions using MULTIVARIATEAPART package [103]. We find,

---

[1] We refer to ref. [77] for the detailed discussion on the construction of the momentum twistor variables $\vec{t}$. In our computation, we perform univariate partial fraction decomposition with respect to x_{1523} variable.

$0 \to \bar{t}tggg$	*before* univariate partial fraction decomposition	*after* univariate partial fraction decomposition
$A_{g;1}^{(1),N_c}\left(1_{\bar{t}}^+, 2_t^+, 3_g^-, 4_g^+, 5_g^+\right)$	78	17
$A_{g;3}^{(1),1}\left(1_{\bar{t}}^+, 2_t^+, 3_g^-, 4_g^+, 5_g^+\right)$	105	30
$0 \to \bar{t}tgg\gamma$	*before* univariate partial fraction decomposition	*after* univariate partial fraction decomposition
$B_{g;1}^{(1),N_c}\left(1_{\bar{t}}^+, 2_t^+, 3_g^+, 4_g^+, 5_g^-\right)$	78	12
$B_{g;1}^{(1),1/N_c}\left(1_{\bar{t}}^+, 2_t^+, 3_g^+, 4_g^+, 5_g^-\right)$	99	28

Table 1: Maximal numerator degrees of the rational coefficients of the pentagon function for the most complicated leading- and subleading- colour contributions in $0 \to \bar{t}tggg$ and $0 \to \bar{t}tgg\gamma$ processes. The degrees are given for the stages *before* and *after* univariate partial fraction decomposition is performed.

however, that the resulting expressions are significantly larger than those prior to multivariate partial fractioning, which subsequently leads to slower numerical evaluation. Hence, we publish our analytic expressions as obtained directly from the analytic reconstruction without performing any further partial fraction decomposition. Finally, it is worth noting that the two processes, $t\bar{t}j$ and $t\bar{t}\gamma$, are related to each other and some of the rational functions might be shared between them. However, such relations can only be fully extracted at the level of primitive amplitude [26]. Nevertheless, using analytic expressions provided in this work, we can explore the connection between the two processes by searching for linear relations among rational coefficients and see how many of the rational coefficients in $t\bar{t}j$ are contained in $t\bar{t}\gamma$, and vice versa. This study is, however, beyond the scope of the present paper.

3 Feynman integrals

In this section, we illustrate the Feynman integral families required for the computation of the one-loop $pp \to t\bar{t}\gamma$ and $pp \to t\bar{t}j$ scattering amplitudes. We employ the uniform transcendental basis of MIs introduced in ref. [66] to derive DEs [56–60] in canonical form [61]. We use the method of pentagon functions [62–64, 104], which has proven to be extremely useful in the computation of 2-loop 5-point massless amplitudes and recently for the computation of 2-loop 5-point amplitudes with massive internal propagators [70, 105]. The same approach was applied also for the computation up to $\mathcal{O}(\epsilon^2)$ of the 1-loop scattering amplitude of $t\bar{t}W$ production [79]. In line with these results, we express the one-loop $pp \to t\bar{t}\gamma$ and $pp \to t\bar{t}j$ scattering amplitudes up to $\mathcal{O}(\epsilon^2)$ in terms of pentagon functions, derive their DEs, and solve them numerically utilizing the generalized series expansion method [81].

In section 3.1, we introduce the notation and define the relevant integral families for the present calculation. In section 3.2, we briefly review the pentagon functions method, and in section 3.4, we discuss the numerical evaluation of the pentagon-function basis. This evaluation is carried out both using the MATHEMATICA package DIFFEXP [82] and the newly available C/C++ package LINE [83].

3.1 Definition of the integral families

The integral families required for the computation of the one-loop $pp \to t\bar{t}\gamma$ and $pp \to t\bar{t}j$ amplitudes can be collectively described by the formula

$$I^{\phi}_{n_1 n_2 n_3 n_4 n_5} = \int \frac{\mathrm{d}^d k_1}{i \pi^{d/2}} \frac{e^{\epsilon \gamma_E}}{D^{n_1}_{\phi,1} D^{n_2}_{\phi,2} D^{n_3}_{\phi,3} D^{n_4}_{\phi,4} D^{n_5}_{\phi,5}}, \tag{43}$$

where $d = 4 - 2\epsilon$ is the space-time dimension and $\phi \in \{P_A, P_B, P_C, P_D\}$. The inverse propagators $D_{\phi,i}$ are defined according to the conventions in ref. [66], and are listed in table 2 for the standard permutation $\sigma_0 = (1, 2, 3, 4, 5)$, where the standard permutation refers to the ordering of the external momenta shown in fig. 2. We recall that labels 1 and 2 refer to the top and antitop quarks, respectively, while 3, 4, and 5 label the external massless particles. In fig. 2, each topology relevant to this computation is illustrated for the standard permutation, σ_0. However, to compute the squared amplitude, it is necessary to include contributions from the same topologies with the external gluons permuted. In particular, the relevant permutations are

$$\sigma \in \{(3, 4, 5), (3, 5, 4), (4, 3, 5), (4, 5, 3), (5, 3, 4), (5, 4, 3)\}, \tag{44}$$

where the fixed pair $(1, 2)$ is omitted for brevity.

	P_A	P_B	P_C	P_D
$D_{\phi,1}$	k_1^2	k_1^2	$k_1^2 - m_t^2$	$k_1^2 - m_t^2$
$D_{\phi,2}$	$(k_1 - p_1)^2 - m_t^2$	$(k_1 - p_1)^2 - m_t^2$	$(k_1 - p_1)^2$	$(k_1 - p_1)^2$
$D_{\phi,3}$	$(k_1 - p_{12})^2$	$(k_1 - p_{13})^2 - m_t^2$	$(k_1 - p_{13})^2$	$(k_1 - p_{12})^2 - m_t^2$
$D_{\phi,4}$	$(k_1 + p_{45})^2$	$(k_1 + p_{45})^2$	$(k_1 + p_{45})^2 - m_t^2$	$(k_1 + p_{45})^2 - m_t^2$
$D_{\phi,5}$	$(k_1 + p_5)^2$	$(k_1 + p_5)^2$	$(k_1 + p_5)^2 - m_t^2$	$(k_1 + p_5)^2 - m_t^2$

Table 2: Inverse propagators $D_{\phi,i}$ for the main permutation of the families contributing to the one-loop $pp \to t\bar{t}\gamma$ and $pp \to t\bar{t}j$ amplitudes. The shorthand notation $p_{i\ldots j} = p_i + \ldots + p_j$ is used for convenience.

By employing LITERED [106] for the generation of IBP identities [53–55] and FINITE-FLOW [84] for solving them, we find for the integral families of type P_A, P_B, P_C, and P_D a set of 15, 17, 19 and 21 MIs, respectively, in agreement with ref. [77]. Furthermore, by utilizing LITERED for obtaining mappings between the MIs of all families, including permutations, we identified a minimal set of 130 MIs, in terms of which the one-loop $pp \to t\bar{t}\gamma$ and $pp \to t\bar{t}j$ amplitudes can be expressed.

By using the bases of integrals provided in ref. [77], which are normalised to be free of ϵ-poles, we construct canonical DEs for the standard permutations, σ_0, of all families, as well as for all the relevant permutations, σ. In particular, for the vector of uniform transcendental MIs of each family, $\vec{g}_{\phi,\sigma}(\vec{x})$, we obtain DEs of the form

$$\mathrm{d}\vec{g}_{\phi,\sigma}(\vec{x}) = \epsilon \, \mathrm{d}A_{\phi,\sigma}(\vec{x}) \, \vec{g}_{\phi,\sigma}(\vec{x}), \tag{45}$$

where the connection matrix, $\mathrm{d}A_{\phi,\sigma}(\vec{x})$, is written in dlog-form

$$\mathrm{d}A_{\phi,\sigma}(\vec{x}) = \sum_{i=1}^{283} a^{(i)}_{\phi,\sigma} \, \mathrm{dlog} \, W_i(\vec{x}). \tag{46}$$

(a) Family P$_A$.

(b) Family P$_B$.
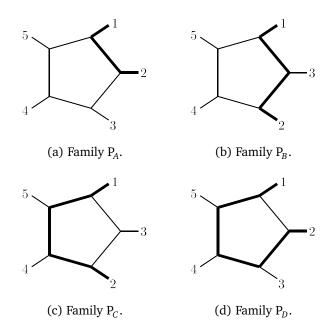
(c) Family P$_C$.

(d) Family P$_D$.

Figure 2: Graphical representation of the standard permutation of the four families contributing to the one-loop $pp \to t\bar{t}\gamma$ and $pp \to t\bar{t}j$ amplitudes. Thin black lines represent massless particles, while thick lines represent the top-quark.

We remind that $\vec{x}$ is the vector of kinematic invariants defined in eq. (7). In eq. (46), $a^{(i)}_{\phi,\sigma}(\vec{x})$ are matrices of rational numbers, $W_i(\vec{x})$ are algebraic functions of $\vec{x}$, known as letters, and the total set of letters is referred to as alphabet. To construct the alphabet across all families and their permutations, we start from the set of letters associated with the standard permutation of each family, as derived in [77]. We then generate all corresponding sets under the kinematic permutations listed in eq. (44) and take their union obtaining an over-complete alphabet. We then identify linear relations among the dlogs of the resulting letters to determine a minimal set of letters. We find 283 independent letters, of which 88 are rational functions of the kinematics, while the remaining ones are algebraic. The alphabet contains a total of 29 independent square roots, which we list in appendix B.

3.2 Pentagon-function basis

In amplitude computations, the ϵ-pole structure is compared with the UV renormalisation and IR subtraction in order to obtain a consistency check as well as to extract the finite reminder. This requires Laurent expanding the scattering amplitude in ϵ, which consequently involves Laurent expansion of the MIs contributing to it. In general, the components of the ϵ-expansion of the MIs are not linearly independent, while it is desirable to express the amplitude in terms of a minimal set of algebraically independent components. The latter leads to significant simplifications in the final expression of the amplitude, to the analytic subtraction of ϵ-poles, and improves the efficiency of the numerical evaluation. In this computation, we consider the components of the ϵ-expansion of the MIs up to ϵ^4, in order to retain all necessary information for future computations of the two-loop finite remainder for the processes addressed. We refer to the basis spanned by the independent components of the MIs as pentagon functions, reflecting the method's initial application to $2 \to 3$ scattering processes. However, we note that the procedure can be generalized to amplitudes with any number of external particles, e.g. [107–109].

To construct a pentagon-function basis related to a given set of MIs, one needs canonical

DEs for the MIs and numerical boundary conditions for them. For the former, in section 3.1, we discussed how we obtained the canonical DEs for all the relevant families ϕ and permutations σ. For the latter, in order to determine the numerical boundary values of the MIs, we evaluate them at an arbitrary point of the physical phase space, $\vec{x}_0$, using AMFlow [110] interfaced to LiteRed and FiniteFlow for the IBP reduction. The AMFlow package utilizes the auxiliary mass flow method [111] for the numerical evaluation of MIs. We evaluate the MIs at $\vec{x}_0$ asking for 70-digit precision. This level of precision exceeds what is expected to be necessary for future applications, but it is employed here since evaluating the MIs at a single point with AMFlow does not constitute a computational bottleneck.

With the above input, the procedure for creating the pentagon-function basis is straightforward. In the following, we provide only a sketch of the procedure; more comprehensive explanations can be found in refs. [37, 62–64, 79, 104]. First, we Laurent expand the MIs around $\epsilon = 0$, so that

$$\vec{g}_{\phi,\sigma}(\vec{x}, \epsilon) = \sum_{\omega=0}^{4} \epsilon^\omega \vec{g}_{\phi,\sigma}^{(\omega)}(\vec{x}) + \mathcal{O}(\epsilon^5), \tag{47}$$

where ω is the order of the expansion, $\vec{g}_{\phi,\sigma}^{(\omega)}(\vec{x})$ the components (of the expansion) of the MIs, and terms of order higher than ϵ^4 are neglected. Then, we iteratively integrate the canonical DEs order by order in ϵ along a path $\gamma : [0, 1] \rightarrow \gamma(t)$ connecting the initial point $\vec{x}_0$ to an arbitrary point of the phase space $\vec{x}$. The solution of the DEs can be written in terms of Chen iterated integrals [112],

$$\vec{g}_{\phi,\sigma}^{(\omega)}(\vec{x}) = \sum_{\omega'=0}^{\omega} \sum_{i_1,i_2,\ldots,i_{\omega'}=1}^{283} a_{\phi,\sigma}^{(i_{\omega'})} a_{\phi,\sigma}^{(i_{\omega'-1})} \ldots a_{\phi,\sigma}^{(i_1)} \vec{g}_{\phi,\sigma}^{(\omega-\omega')}(\vec{x}_0) \left[W_{i_1}, W_{i_2}, \ldots, W_{i_{\omega'}} \right]_{\vec{x}_0}(\vec{x}), \tag{48}$$

where

$$\left[W_{i_1}, W_{i_2}, \ldots, W_{i_\omega} \right]_{\vec{x}_0}(\vec{x}) \equiv \int_0^1 dt \, \frac{\partial \log W_{i_\omega}(\gamma(t))}{\partial t} \left[W_{i_1}, W_{i_2}, \ldots, W_{i_{\omega-1}} \right]_{\vec{x}_0}(\gamma(t)), \tag{49}$$

with $[\,]_{\vec{x}_0}(\vec{x}) = 1$ for $\omega = 0$. In this case, the order of the expansion ω also represents the transcendental weight, which counts the number of iterated integrations. A very useful property of Chen iterated integrals is that they form a shuffle algebra. This means that the product of an iterated integral of weight ω_1 with an iterated integral of weight ω_2 can be expressed as a sum of iterated integrals of weight $\omega_1 + \omega_2$ according to the equation

$$\left[W_{a_1}, \ldots, W_{a_{\omega_1}} \right]_{\vec{x}_0}(\vec{x}) \left[W_{b_1}, \ldots, W_{b_{\omega_2}} \right]_{\vec{x}_0}(\vec{x}) = \sum_{\vec{c}=\vec{a} \shuffle \vec{b}} \left[W_{c_1}, \ldots, W_{c_{\omega_1+\omega_2}} \right]_{\vec{x}_0}(\vec{x}), \tag{50}$$

where $\vec{a}, \vec{b}, \vec{c}$ are index vectors, and $\vec{a} \shuffle \vec{b}$ denotes all possible ways to shuffle the indices of $\vec{a}$ and $\vec{b}$ while preserving the order within each vector.

We proceed by identifying the relations among MIs at the symbol level [113–115]. These relations can then be lifted to the iterated integrals based on the ansatz, proposed in ref. [104], that only terms proportional to ζ need to be included. This procedure will be briefly reviewed later in the section. For now, we start by finding relations at the symbol level for the 130 independent MIs, denoted by $\vec{g}$. The MIs at symbol level can be written as

$$\mathcal{S}\left[\vec{g}^{(\omega)} \right] = \sum_{\omega'=0}^{\omega} \sum_{i_1,\ldots,i_{\omega'}} a^{(i_{\omega'})} a^{(i_{\omega'-1})} \ldots a^{(i_1)} \vec{g}^{(\omega-\omega')}(\vec{x}_0) W_{i_1} \otimes W_{i_2} \otimes \ldots \otimes W_{i_{\omega'}}. \tag{51}$$

Weight	0	1	2	3	4	all
pentagon functions	1	15	53	111	101	281

Table 3: Number of pentagon functions at each weight used in the computation of the full colour one-loop scattering amplitude up to $\mathcal{O}(\epsilon^2)$ for the processes $pp \to t\bar{t}\gamma$ and $pp \to t\bar{t}j$.

Next, we identify the algebraically independent components of the MIs, weight by weight. At weight zero, we have only rational numbers, which can be written in terms of a single constant that we define as $F^{(0)} = 1$, where $F^{(0)}$ represents the pentagon function at weight zero. At weight one, we can derive the $\mathcal{Q}$-linear relations through the condition

$$\sum_{i=1}^{130} c_i \, \mathcal{S}\left[g_i^{(1)}\right] = 0 \,. \tag{52}$$

The procedure for higher weights is similar but not identical. More specifically, for weights $\omega \geq 2$, we must also consider, in the ansatz of eq. (52), products of lower-weight pentagon functions, which take the form

$$F_{i_1}^{(\omega_1)} F_{i_2}^{(\omega_2)} \ldots F_{i_k}^{(\omega_k)} \,, \tag{53}$$

with $\omega_1 + \omega_2 + \ldots + \omega_k = \omega$ and $1 \leq \omega_i < \omega$ for $i = 1, \ldots, k$ and $1 < k < \omega$. The symbol of the latter can be expressed in terms of weight ω symbols by exploiting shuffle algebra, eq. (50).

Subsequent to this step, the relations between the symbols of the ansatz can be found in the same manner as was done for the weight one case. Since the choice of independent MI components forming the pentagon function basis is arbitrary, we tune the ordering so that products of lower-weight pentagon functions are preferred over higher-weight ones. This helps minimize the number of higher-weight pentagon functions that appear in the basis. The number of independent pentagon functions at each weight is summarized in table 3.

The last step consists of expressing the components of the MIs in terms of the constructed basis of pentagon functions. To do so, products of lower weight pentagon functions and transcendental constants with vanishing symbols need to be added in the ansatz defining the MI components in terms of pentagon functions. Therefore $\vec{g}^{(k)}(\vec{x})$ are expressed as polynomials in the basis of pentagon functions and the transcendental constants ζ_2 and ζ_3, with rational numbers as coefficients, as proposed in ref. [104]. For example, at weight two, we can make the ansatz

$$\vec{g}^{(2)}(\vec{x}) = \sum_i c^i F_i^{(2)} + \sum_{i,j} c^{i,j} F_i^{(1)} F_j^{(1)} + \tilde{c} \, \zeta_2 \,, \tag{54}$$

where the rational numbers c^i and $c^{i,j}$ are already known from the symbol-level analysis. The coefficient $\tilde{c}$ can be determined by ensuring consistency with the expression of the MI components in terms of Chen iterated integrals, as outlined in eq. (48). More specifically, the right-hand side of eq. (54) is set equal to the right-hand side of eq. (48) at weight two, where the pentagon functions are expressed in terms of MI components and subsequently in terms of Chen iterated integrals. By utilizing the linear independence of the iterated integrals, we obtain a system of linear equations consisting of the boundary values $\{\vec{g}^{(0)}(\vec{x}_0), \vec{g}^{(1)}(\vec{x}_0), \vec{g}^{(2)}(\vec{x}_0)\}$ and the undetermined coefficients. Given that the boundary values are already computed using AMFLOW, we can determine the coefficient $\tilde{c}$ only numerically, and then we rationilize their values. To verify the correctness of this result, we evaluate the left-hand side of eq. (54), including the contribution of the $\tilde{c} \, \zeta_2$ term, at a random point in the physical phase space using

AMFLOW to obtain the values of the pentagon functions. We then compare this result with the numerical evaluation of the corresponding MI components on the right-hand side of eq. (54), also performed with AMFLOW. This comparison is carried out at five different phase-space points.

Proceeding in a similar way at each weight, we express all the MI components as polynomials with rational coefficients in the algebraically independent MI components, denoted as $\{F_i^{(k)}\}$ and known as the pentagon function basis, including also the transcendental constants $\{\zeta_2, \zeta_3\}$. For example, the weight-two component of MI 36 is written as

$$\vec{g}_{36}^{(2)}(\vec{x}) = -\zeta_2 + 4F_1^{(1)}F_5^{(1)} - F_3^{(1)}F_5^{(1)} - 3\left(F_5^{(1)}\right)^2 + F_5^{(1)}F_7^{(1)} + 2F_5^{(1)}F_8^{(1)} \tag{55}$$
$$+ 2F_5^{(1)}F_{11}^{(1)} - 2F_5^{(1)}F_{13}^{(1)} + F_{20}^{(2)}.$$

The analytic expressions of the MI components in terms of the pentagon functions are reported in the ancillary file `anc/specialfunc/SFbasis/MIs_to_SFs.m` [102].

3.3 Physical region

We focus on the s_{34} scattering channel ($34 \rightarrow 125$), since the other channels relevant to the production processes $pp \rightarrow t\bar{t}\gamma$ and $pp \rightarrow t\bar{t}j$ can be derived by performing an appropriate permutation of the external momenta. We will describe how to handle these permutations in a next section. In the physical region, the momenta are required to be real and associated with physical scattering angles and positive energies. For the s_{34} channel, this translates into the following conditions

$$p_1^2 > 0, \quad p_2^2 > 0, \quad p_3 \cdot p_4 > 0, \quad p_1 \cdot p_2 > 0, \quad p_1 \cdot p_5 > 0, \quad p_2 \cdot p_5 > 0,$$
$$p_1 \cdot p_3 < 0, \quad p_2 \cdot p_3 < 0, \quad p_3 \cdot p_5 < 0, \quad p_1 \cdot p_4 < 0, \quad p_2 \cdot p_4 < 0, \quad p_4 \cdot p_5 < 0. \tag{56}$$

Additionally, the following Gram determinant constraints must be satisfied [116, 117]

$$\det G(p_i, p_j) < 0, \qquad \det G(p_i, p_j, p_k) > 0, \qquad \det G(p_i, p_j, p_k, p_l) < 0, \tag{57}$$

where $\{i, j, k, l\} \in \{1, \ldots, 5\}$. We refer to appendix B for the definition of the Gram determinant. These conditions, together with the previously stated constraints, impose a set of polynomial relations on the kinematic invariants that define the boundary of our physical region. These constrains can be found in the ancillary file `anc/specialfunc/DiffExpRun/s34_-channel.m` [102]. We comment that for the square roots with negative argument, we choose to have positive imaginary part.

3.4 Numerical evaluation of the pentagon functions

To enable analytic cancellation of the poles in the finite remainder, we have derived analytic expressions in terms of logarithms for the weight-one pentagon functions, in order to express the IR subtraction and UV factorisation terms in the same basis of functions as the amplitude.

The analytic expressions are the following

$$F_1^{(1)} = \log\left(\frac{2(d_{12} + d_{23} - d_{45} + m_t^2)}{m_t^2}\right),$$

$$F_2^{(1)} = \frac{\log(m_t^2)}{2} + \log\left(\frac{d_{15} - d_{23} + d_{45}}{d_{34} + d_{45} - d_{12} - m_t^2}\right) - 2\log\left(2(d_{34} - d_{12} - d_{15} - m_t^2)\right) + 2i\pi,$$

$$F_3^{(1)} = \frac{\log(m_t^2)}{2} + \log\left(\frac{d_{34} - d_{12} - d_{15} - m_t^2}{d_{34}}\right) - 2\log\left(2(d_{15} - d_{23} + d_{45})\right),$$

$$F_4^{(1)} = \frac{\log(m_t^2)}{2} - \log\left(\frac{d_{34} - d_{12} - d_{15} - m_t^2}{d_{34}}\right) - \log\left(2(d_{12} + m_t^2)\right) + i\pi,$$

$$F_5^{(1)} = \log\left(2(d_{34} - d_{12} - d_{15} - m_t^2)\right) - \log(m_t^2) - i\pi,$$

$$F_6^{(1)} = \frac{\log(m_t^2)}{2} + \log\left(\frac{d_{12} + d_{23} - d_{45} + m_t^2}{d_{45}}\right) - 2\log\left(2(d_{34} - d_{12} - d_{15} - m_t^2)\right) + 2i\pi,$$

$$F_7^{(1)} = \frac{\log(m_t^2)}{2} + \log\left(\frac{d_{34} - d_{12} - d_{15} - m_t^2}{d_{34}}\right) - 2\log\left(2(d_{12} + d_{23} - d_{45} + m_t^2)\right),$$

$$F_8^{(1)} = \frac{\log(m_t^2)}{2} + \log\left(\frac{d_{23} + d_{34} - d_{15}}{d_{12} + d_{23} - d_{45} + m_t^2}\right) - \log\left(2d_{15}\right) + i\pi, \tag{58}$$

$$F_9^{(1)} = -\log\left(\frac{2(d_{12} + d_{23} - d_{45} + m_t^2)}{m_t^2}\right) - \log\left(-2d_{23}\right),$$

$$F_{10}^{(1)} = \log\left(-\frac{1 + r_{24}}{1 - r_{24}}\right),$$

$$F_{11}^{(1)} = \log(m_t^2) - \log\left(2(d_{23} + d_{34} - d_{15})\right) - \log\left(2(d_{15} - d_{23} + d_{45})\right),$$

$$F_{12}^{(1)} = \log\left(-\frac{1 + r_{25}}{1 - r_{25}}\right),$$

$$F_{13}^{(1)} = \log(m_t^2) - \log\left(2(d_{34} - d_{12} - d_{15} - m_t^2)\right) - \log\left(2d_{15}\right) + 2i\pi,$$

$$F_{14}^{(1)} = \log\left(-\frac{1 + r_{27}}{1 - r_{27}}\right) - i\pi,$$

$$F_{15}^{(1)} = -\log\left(-\frac{1 + r_4}{1 - r_4}\right) + i\pi,$$

where all the logarithms are well defined in the s_{34} channel.

We do not derive explicit expressions for pentagon functions of higher weights. Instead, we provide tailored procedures for their numerical evaluation. To achieve this, we construct a system of linear DEs for evaluating the basis of pentagon functions [37]. The DEs take the form

$$\mathrm{d}\,\vec{G}(\vec{x}) = \tilde{A}(\vec{x})\,\vec{G}(\vec{x}), \tag{59}$$

with the connection matrix having the standard dlog-form

$$\tilde{A}(\vec{x}) = \sum_i \tilde{a}_i \, \mathrm{dlog}\, W_i(\vec{x}). \tag{60}$$

Here, $\vec{G}(\vec{x})$ represents the minimal set of pentagon functions necessary to construct the linear DEs.

Let us now illustrate the procedure of finding the minimal basis $\vec{G}(\vec{x})$ and creating the aforementioned DEs. We begin by considering the weight-four pentagon functions, denoted

as $\{F_i^{(4)}\}$. We compute their derivatives with respect to the kinematic invariants, leveraging the knowledge of DEs for the MIs. Indeed, the pentagon functions $\{F_i^{(4)}\}$ are by definition MIs components, i.e. $\vec{g}^{(4)}(\vec{x})$, whose derivatives are given by the ϵ-expansion of eq. (45). The derivatives of the weight-four functions will only involve weight-three functions, including products of lower-weight functions whose total weight is equal to three. To obtain a closed system of DEs, we include these products in the set $\vec{G}(\vec{x})$, along with the weight-three pentagon functions $\{F_i^{(3)}\}$, and differentiate them accordingly. To ensure that we solve the DEs for a minimal set of functions $\vec{G}(\vec{x})$, we restrict the set of functions to only the independent linear combinations of lower weight products that appear in the DEs. This process is repeated at each weight until we reach weight zero. Upon completion, we obtain DEs for a total of 325 functions, which represents an extension of the original basis of pentagon functions $\{F_i^{(w)}\}$. The set of pentagon functions $\vec{G}(\vec{x})$ together with their DEs can be found in the ancillary file `anc/specialfunc/SFBasis/SF_DEs.m` [102].

The boundary values for the set of pentagon functions $\vec{G}(\vec{x})$ are determined using numerical evaluations of the MIs performed with AMFLOW, requesting a precision of 70 digits. We provide the values of $\vec{G}(\vec{x})$ in four different phase-space points in the ancillary files `anc/specialfunc/DiffExpRun/Bounds/AMF_X#.m` [102], with $\# = 1, 2, 3, 4$. These points are chosen to lie in the s_{34} channel, defined in section [?], and are randomly generated with the only constraint being to avoid spurious singularities in the DEs. The boundary values provided have been used to solve the DEs. The propagation of the solution from one of these benchmark points to another using the generalized series expansion [81], as implemented in DIFFEXP [82], served as a cross-check of the DEs. In `anc/specialfunc/DiffExpRun/DiffExp_ttA.wl` file [102] one can find our DIFFEXP setup. This setup can be employed to evaluate the solution of the DEs for any target point connected to a boundary point by a path that lies entirely within the s_{34} channel. The integration path may, in principle, extend beyond the physical region; however, this would require crossing branch cuts associated with physical singularities. In such cases, an appropriate analytic continuation prescription must be supplied to the DE solver. To circumvent this complication, for target points not directly connected to the available boundary conditions within the physical region, an intermediate point connected to both a boundary point and the target can be introduced. The special functions evaluated at this intermediate point then serve as boundary conditions for propagating the DEs solution to the target point. Furthermore, we observe that starting from the four phase-space points at which the special functions are provided in the ancillary files, our numerical implementation provides coverage of the entire physical region. This test has been perfomed for $100k$ phase-space points generated with `MadGraph5` [72] for $pp \to t\bar{t}\gamma$ at LO.

Additionally to the DIFFEXP implementation for the solution of the pentagon-function DEs, we provide also an implementation in terms of the newly available LINE package [83]. Since LINE can only handle connection matrices with rational functions, it is necessary to rotate the DEs to eliminate square roots from the connection matrices. We perform this rotation using the transformation rule

$$\vec{G}'(\vec{x}) = N \, \vec{G}(\vec{x}) \qquad \text{and} \qquad \tilde{A}'(\vec{x}) = N \tilde{A}(\vec{x}) N^{-1} + \mathrm{d}N \, N^{-1}, \qquad (61)$$

where the normalisation matrix N is chosen such that the connection matrix $\tilde{A}'(\vec{x})$ is square-root free. In particular, we construct N so as to multiply the pentagon functions that are associated with MIs containing square roots in their normalization by the corresponding square roots. LINE is used for solving the DEs of $\vec{G}'(\vec{x})$ and the solution of $\vec{G}(\vec{x})$ is obtained by using the inverse transformation. A script to rotate the DEs and prepare inputs for running LINE is provided in the ancillary file `anc/specialfunc/LINErun/LINEinput_ttA.wl` [102].

We emphasize that the basis for the pentagon functions has been constructed to include all permutations of the three external massless particles in eqs. (1) to (4). This ensures that

all colour configurations, shown in eqs. (9), (11), (15) and (17), as well as all helicity configurations necessary for evaluating the squared amplitudes of all the channels relevant for $t\bar{t}j$ and $t\bar{t}\gamma$ production in pp collisions are covered. Thanks to this construction, once the DEs are solved, there is no need to re-evaluate the pentagon functions or perform any analytic continuation when permuting external legs to obtain other helicity or colour configurations beyond the independent ones. Everything is already embedded in the solution. To illustrate this, consider the evaluation of the pentagon function $F_2^{(1)}(\vec{x})$ at a phase-space point corresponding to the permutation

$$\sigma' : (p_1, p_2, p_3, p_4, p_5) \to (p_1, p_2, p_3, p_5, p_4). \tag{62}$$

We can derive the relation

$$F_2^{(1)}(\sigma' \cdot \vec{x}) = \sigma' \cdot F_2^{(1)}(\vec{x}) = \sigma' \cdot g_{2,\phi,\sigma}^{(1)}(\vec{x}) = g_{2,\phi,\sigma' \cdot \sigma}^{(1)}(\vec{x}) = F_7^{(1)}(\vec{x}) - 2F_8^{(1)}(\vec{x}) + F_{13}^{(1)}(\vec{x}). \tag{63}$$

This means that the evaluation of $F_2^{(1)}(\vec{x})$ at the permuted kinematic point can be obtained from a specific linear combination of pentagon functions evaluated at the original (non-permuted) point, which we choose to lie in the s_{34} channel. In the file `anc/specialfunc/SFbasis/SFs_-perm_rule.m` [102], we provide a list of permutation rules for the pentagon functions.

We further carried out performance studies for numerical evaluations using LINE and DIFFEXP. The timings were measured on 100 physical phase-space points,[2] and we found that, on average, LINE is about twice as fast as DIFFEXP in propagating solutions of the DEs while aiming for the same number of digits of accuracy in the results. Beyond speed, an additional advantage of LINE over DIFFEXP for large-scale cluster evaluations is that it does not require a MATHEMATICA license. Additionally, we also compared numerical evaluations based on the generalized series expansion method between the master-integral and pentagon-function representations. The system of DEs for the MIs associated with one of the families in ϕ at a given permutation is significantly smaller, since it involves only a single permutation, whereas the pentagon functions cover the full set of permutations and families. However, for a given phase-space point, the numerical solutions for the MIs have to be computed multiple times (once for each permutation), while in the pentagon-function representation they are evaluated only once. We tested this using DIFFEXP on a few physical phase-space points and found the timings to be comparable between the two approaches. We note, however, that the computational advantage of the pentagon-function representation, in terms of evaluation speed, typically arises when employing one-fold integral representations [63, 64, 118], which we leave for future work.

4   Numerical benchmark results

In this section, we employ the analytic expressions of the helicity amplitudes, together with the special function basis to obtain numerical results for colour- and helicity-summed UV renormalised squared amplitudes. For $pp \to t\bar{t}j$ production, we consider the following partonic scattering channels for the $0 \to \bar{t}tggg$ process,

$$gg \to \bar{t}tg : \quad g(-p_3) + g(-p_4) \to \bar{t}(p_1) + t(p_2) + g(p_5), \tag{64}$$

---

[2]We restricted to points that can be connected to the boundary point by a path that does not cross singularities. In the current version of LINE, crossing singularities requires manual tuning of the working precision for each run by trial and error, which we chose not to pursue in this analysis.

and for the $0 \to \bar{t}t\bar{q}qg$ process we have

$$
\begin{align}
u\bar{u} \to \bar{t}tg : \quad & u(-p_3) + \bar{u}(-p_4) \to \bar{t}(p_1) + t(p_2) + g(p_5), \tag{65a}\\
\bar{u}u \to \bar{t}tg : \quad & \bar{u}(-p_3) + u(-p_4) \to \bar{t}(p_1) + t(p_2) + g(p_5), \tag{65b}\\
ug \to \bar{t}tu : \quad & u(-p_3) + g(-p_4) \to \bar{t}(p_1) + t(p_2) + u(p_5), \tag{65c}\\
\bar{u}g \to \bar{t}t\bar{u} : \quad & \bar{u}(-p_3) + g(-p_4) \to \bar{t}(p_1) + t(p_2) + \bar{u}(p_5), \tag{65d}\\
gu \to \bar{t}tu : \quad & g(-p_3) + u(-p_4) \to \bar{t}(p_1) + t(p_2) + u(p_5), \tag{65e}\\
g\bar{u} \to \bar{t}t\bar{u} : \quad & g(-p_3) + \bar{u}(-p_4) \to \bar{t}(p_1) + t(p_2) + \bar{u}(p_5). \tag{65f}
\end{align}
$$

For $pp \to t\bar{t}\gamma$ production, there is one partonic channel for $0 \to \bar{t}tgg\gamma$ process,

$$
gg \to \bar{t}t\gamma : \quad g(-p_3) + g(-p_4) \to \bar{t}(p_1) + t(p_2) + \gamma(p_5), \tag{66}
$$

while there are four channels in the $0 \to \bar{t}t\bar{q}q\gamma$ process,

$$
\begin{align}
u\bar{u} \to \bar{t}t\gamma : \quad & u(-p_3) + \bar{u}(-p_4) \to \bar{t}(p_1) + t(p_2) + \gamma(p_5), \tag{67a}\\
d\bar{d} \to \bar{t}t\gamma : \quad & d(-p_3) + \bar{d}(-p_4) \to \bar{t}(p_1) + t(p_2) + \gamma(p_5), \tag{67b}\\
\bar{u}u \to \bar{t}t\gamma : \quad & \bar{u}(-p_3) + u(-p_4) \to \bar{t}(p_1) + t(p_2) + \gamma(p_5), \tag{67c}\\
\bar{d}d \to \bar{t}t\gamma : \quad & \bar{d}(-p_3) + d(-p_4) \to \bar{t}(p_1) + t(p_2) + \gamma(p_5). \tag{67d}
\end{align}
$$

To present a benchmark numerical evaluation, we employ the following randomly chosen physical phase-space point (given in the units of GeV) that lies in the $34 \to 125$ channel,

$$
\begin{align}
p_1 &= (421.812558294, 72.3820876039, 342.337070428, 163.070530566), \\
p_2 &= (463.866064984, -151.62473585, -322.765175691, -243.113773948), \\
p_3 &= (-500, 0, 0, -500), \tag{68}\\
p_4 &= (-500, 0, 0, 500), \\
p_5 &= (114.321376722, 79.2426482461, -19.5718947366, 80.0432433819),
\end{align}
$$

which corresponds to the value of top-quark mass of $m_t = 170$ GeV, together with the following coupling constants, renormalisation scale and parameters,

$$
\alpha_s = 0.118, \qquad \alpha = \frac{1}{137}, \qquad \mu_R = 1 \text{ GeV}, \quad n_f = 5, \quad n_h = 1. \tag{69}
$$

Additionally, lightlike reference vectors entering the definition of massive spinors in eq. (30) are arbitrarily chosen to be

$$
\begin{align}
n_1 &= (3, 2, 2, 1), \\
n_2 &= (3, 2, 1, 2). \tag{70}
\end{align}
$$

In tables 4 and 5, we present numerical results for the the colour- and helicity-summed one-loop amplitude interfered with the tree-level amplitude, normalised with respect to the tree-level amplitude as

$$
\frac{2\mathrm{Re}\sum \mathcal{M}^{(0)*}\mathcal{M}^{(1)}}{\frac{\alpha_s}{4\pi}\sum |\mathcal{M}^{(0)}|^2}, \tag{71}
$$

evaluated at the phase-space point given in eq. (68). These results have been validated against OPENLOOPS [76] up to $\mathcal{O}(\epsilon^0)$. In the MATHEMATICA notebook that we provide to evaluate the squared matrix elements for both $t\bar{t}j$ and $t\bar{t}\gamma$ production, the numerical entries for the momenta are given to 100-digit precision, while the numerical values of the pentagon function basis have been computed with LINE to an accuracy of 32 digits.

$0 \to \bar{t}tggg$	ϵ^{-2}	ϵ^{-1}	ϵ^{0}	ϵ^{1}	ϵ^{2}
$gg \to \bar{t}tg$	-18.000000	196.49906	-1289.8912	4852.8064	-13717.358

$0 \to \bar{t}t\bar{q}qg$	ϵ^{-2}	ϵ^{-1}	ϵ^{0}	ϵ^{1}	ϵ^{2}
$u\bar{u} \to \bar{t}tg$	-11.333333	119.80952	-872.01453	3501.7374	-11272.732
$\bar{u}u \to \bar{t}tg$	-11.333333	114.02910	-798.36940	3030.3552	-9278.0196
$ug \to \bar{t}tu$	-11.333333	134.05316	-986.23890	3843.0879	-11171.395
$\bar{u}g \to \bar{t}t\bar{u}$	-11.333333	132.56334	-973.29477	3791.4615	-11047.051
$gu \to \bar{t}tu$	-11.333333	121.80354	-877.87570	3399.8392	-10211.249
$g\bar{u} \to \bar{t}t\bar{u}$	-11.333333	129.14005	-962.56681	3882.2416	-12038.663

Table 4: Numerical results for $pp \to t\bar{t}j$ UV-renormalised one-loop amplitudes interfered with the corresponding tree level amplitudes, normalised according to eq. (71), evaluated at the phase-space point specified in eq. (68).

$0 \to \bar{t}tgg\gamma$	ϵ^{-2}	ϵ^{-1}	ϵ^{0}	ϵ^{1}	ϵ^{2}
$gg \to \bar{t}t\gamma$	-12.000000	149.51298	-1070.6693	4402.2091	-13362.539

$0 \to \bar{t}t\bar{q}q\gamma$	ϵ^{-2}	ϵ^{-1}	ϵ^{0}	ϵ^{1}	ϵ^{2}
$u\bar{u} \to \bar{t}t\gamma$	-5.3333333	71.531343	-631.45963	2904.3524	-10280.372
$d\bar{d} \to \bar{t}t\gamma$	-5.3333333	71.531343	-633.66653	2931.1602	-10440.782
$\bar{u}u \to \bar{t}t\gamma$	-5.3333333	64.932872	-548.72683	2389.0454	-8147.6420
$\bar{d}d \to \bar{t}t\gamma$	-5.3333333	64.932872	-549.43852	2391.3058	-8150.1573

Table 5: Numerical results for $pp \to t\bar{t}\gamma$ UV-renormalised one-loop amplitudes interfered with the corresponding tree level amplitudes, normalised according to eq. (71), evaluated at the phase-space point specified in eq. (68).

5 Conclusions

In this work, we have derived analytic expressions for the full-colour one-loop helicity amplitudes for $t\bar{t}\gamma$ and $t\bar{t}j$ production processes up to $\mathcal{O}(\epsilon^2)$. The motivation behind our computation lies in the growing need for precise scattering amplitudes results, through NNLO accuracy in the perturbative expansion around $\alpha_s = 0$. While several automated tools are available for computing the finite part of one-loop amplitudes, two-loop computations require the one-loop expressions expanded up to $\mathcal{O}(\epsilon^2)$. Our results thus contribute to this goal, while at the same time offering insight into the algebraic complexity of the two-loop scattering amplitudes of $t\bar{t}j$ and $t\bar{t}\gamma$ production.

Within our calculation, we employed a tensor decomposition of the amplitudes in four dimensions [85,86] to derive the helicity-amplitude representation. The algebraic complexity arising from the enormous size of intermediate expressions was managed using finite-field methods [51,52,84]. In order to express the amplitudes in a compact manner, we constructed a basis of pentagon functions [62–64], which is evaluated using generalised series expansion techniques [81]. In this context, we made use of the DIFFEXP package [82] and the newly released LINE package [83], which showed improved performances for our system of DEs. Our results represent a novel contribution for the one-loop scattering amplitude of $t\bar{t}\gamma$ production, while for the corresponding $t\bar{t}j$ case, the derivation of the pentagon function basis marks an advancement over previous computations [77].

The choice of expressing the amplitudes in terms of a pentagon-function basis is motivated not only by the resulting compactness and numerical efficiency of the one-loop expressions but also by the long-term goal of facilitating future two-loop computations of these processes. Previous analyses of leading-colour two-loop amplitudes for $t\bar{t}j$ production have shown that the relevant functional space extends beyond polylogarithmic functions and includes elliptic structures [65–67,70]. As shown in the $t\bar{t}j$ case, although a complete set of independent pentagon functions was not yet available in the general context of elliptic functions, it was possible to construct a potentially overcomplete pentagon functions-like basis. This approach led to several advantages, including the separation of polylogarithmic and non-polylogarithmic contributions, with the latter pushed into the finite part of the amplitude, enabling analytic cancellation of poles and simplification of the amplitude expressions. Furthermore, the construction of this basis improved both numerical stability and efficiency. Given that the same Feynman integral topologies, along with more complex ones, are expected to appear in the two-loop leading-colour $t\bar{t}\gamma$ amplitude, we anticipate that a similar strategy could be effective in this case as well. This, however, remains the subject of future research.

Acknowledgements

A   Renormalisation constants

The required one-loop QCD renormalisation constants are given by [119, 120]

$$\delta Z_m^{(1)} = Z_t^{(1)} = \frac{e^{\epsilon \gamma_E} \Gamma(1+\epsilon)}{(m_t^2)^\epsilon} \, C_F \left(-\frac{3}{\epsilon} - \frac{4}{1-2\epsilon} \right), \tag{72a}$$

$$\delta Z_g^{(1)} = \frac{e^{\epsilon \gamma_E} \Gamma(1+\epsilon)}{(m_t^2)^\epsilon} \, T_F n_h \left(-\frac{4}{3\epsilon} \right), \tag{72b}$$

$$\delta Z_{\alpha_s}^{(1)} = -\frac{\beta_0}{\epsilon} + \frac{4}{3} T_F n_h \left[\frac{1}{\epsilon} - \log(m_t^2) \right], \tag{72c}$$

where for the strong coupling renormalisation counterterm, the n_f light quarks are subtracted using the $\overline{\text{MS}}$ scheme while the heavy quark loop is subtracted at zero momentum. The one-loop β-function coefficient is

$$\beta_0 = \frac{11}{3} C_A - \frac{4}{3} T_F n_f \,, \tag{73}$$

with

$$C_F = \frac{N_c^2 - 1}{2 N_c}, \qquad C_A = N_c \qquad \text{and} \qquad T_F = \frac{1}{2}. \tag{74}$$

B   Independent square roots

In this appendix, we list the independent square roots appearing in the computation of the one-loop $pp \to t\bar{t}\gamma$ and $pp \to t\bar{t}j$ squared amplitudes. The list of square roots is:

$$r_1 = \sqrt{\text{tr}_5^2/4}, \qquad\qquad\qquad r_2 = \sqrt{-\det G(p_2, p_1 + p_5)},$$

$$r_3 = \sqrt{-\det G(p_1, p_2 + p_3)}, \qquad\qquad r_4 = \sqrt{\frac{d_{12} - m_t^2}{d_{12} + m_t^2}},$$

$$r_5 = \sqrt{-\det G(p_2, p_1 + p_4)}, \qquad\qquad r_6 = \sqrt{-\det G(p_1, p_2 + p_5)},$$

$$r_7 = \sqrt{\frac{\det Y_{p_1|p_5|p_2|p_3+p_4}^{0 m_t m_t 0}}{d_{25}^2 d_{15}^2}}, \qquad\qquad r_8 = \sqrt{\frac{\det Y_{p_1+p_3|p_2|p_4|p_5}^{m_t 0 m_t m_t}}{d_{24}^2 d_{45}^2}},$$

$$r_9 = \sqrt{\frac{\det Y_{p_1|p_2+p_3|p_4|p_5}^{m_t 0 m_t m_t}}{d_{15}^2 d_{45}^2}}, \qquad\qquad r_{10} = \sqrt{-\det G(p_2, p_1 + p_3)},$$

$$r_{11} = \sqrt{\frac{\det Y_{p_1+p_3|p_2|p_5|p_4}^{m_t 0 m_t m_t}}{d_{25}^2 d_{45}^2}}, \qquad\qquad r_{12} = \sqrt{\frac{\det Y_{p_1|p_2+p_3|p_5|p_4}^{m_t 0 m_t m_t}}{d_{14}^2 d_{45}^2}},$$

$$r_{13} = \sqrt{\frac{\det Y_{p_2|p_3|p_5|p_1+p_4}^{0 m_t m_t m_t}}{d_{23}^2 d_{35}^2}}, \qquad\qquad r_{14} = \sqrt{\frac{\det Y_{p_1|p_2+p_4|p_3|p_5}^{m_t 0 m_t m_t}}{d_{15}^2 d_{35}^2}},$$

$$r_{15} = \sqrt{-\det G(p_1, p_2 + p_4)}, \qquad\qquad r_{16} = \sqrt{\frac{\det Y_{p_1+p_4|p_2|p_5|p_3}^{m_t 0 m_t m_t}}{d_{25}^2 d_{35}^2}}, \tag{75}$$

$$r_{17} = \sqrt{\frac{\det Y^{m_t 0 m_t m_t}_{p_1|p_2+p_4|p_5|p_3}}{d_{13}^2 d_{35}^2}}, \qquad r_{18} = \sqrt{\frac{\det Y^{0 m_t m_t m_t}_{p_2|p_3|p_4|p_1+p_5}}{d_{23}^2 d_{34}^2}},$$

$$r_{19} = \sqrt{\frac{\det Y^{0 m_t m_t m_t}_{p_2|p_4|p_3|p_1+p_5}}{d_{24}^2 d_{34}^2}}, \qquad r_{20} = \sqrt{\frac{\det Y^{m_t 0 m_t m_t}_{p_1|p_2+p_5|p_3|p_4}}{d_{14}^2 d_{34}^2}},$$

$$r_{21} = \sqrt{\frac{\det Y^{m_t 0 m_t m_t}_{p_1|p_2+p_5|p_4|p_3}}{d_{13}^2 d_{34}^2}}, \qquad r_{22} = \sqrt{\frac{\det Y^{0 m_t m_t 0}_{p_1|p_3|p_2|p_4+p_5}}{d_{23}^2 d_{13}^2}},$$

$$r_{23} = \sqrt{\frac{\det Y^{0 m_t m_t 0}_{p_1|p_4|p_2|p_3+p_5}}{d_{24}^2 d_{14}^2}}, \qquad r_{24} = \sqrt{1 - \frac{2m_t^2}{d_{45}}},$$

$$r_{25} = \sqrt{1 - \frac{2m_t^2}{d_{12} - d_{34} - d_{45} + m_t^2}}, \qquad r_{26} = \sqrt{\frac{\det Y^{m_t m_t m_t m_t}_{p_1+p_2|p_3|p_4|p_5}}{d_{34}^2 d_{45}^2}},$$

$$r_{27} = \sqrt{1 - \frac{2m_t^2}{d_{34}}}, \qquad r_{28} = \sqrt{\frac{\det Y^{m_t m_t m_t m_t}_{p_1+p_2|p_3|p_5|p_4}}{d_{35}^2 d_{45}^2}},$$

$$r_{29} = \sqrt{\frac{\det Y^{m_t m_t m_t m_t}_{p_1+p_2|p_4|p_5|p_3}}{d_{34}^2 d_{35}^2}},$$

with the Gram and Cayley matrices are defined by

$$G(p_1, \cdots, p_n) = \begin{pmatrix} p_1 \cdot p_1 & p_1 \cdot p_2 & \cdots & p_1 \cdot p_n \\ p_2 \cdot p_1 & p_2 \cdot p_2 & \cdots & p_2 \cdot p_n \\ \vdots & \vdots & \ddots & \vdots \\ p_n \cdot p_1 & p_n \cdot p_2 & \cdots & p_n \cdot p_n \end{pmatrix}, \qquad \left[Y^{m_1 m_2 m_3 m_4}_{P_1|P_2|P_3|P_4} \right]_{ij} = \frac{1}{2} \left[(q_i - q_j)^2 - m_i^2 - m_j^2 \right],$$

$$\tag{76}$$

where $q_i = \sum_{k=0}^{i-1} P_k$.

References

[1] U. Husemann, *Top-Quark Physics: Status and Prospects*, Prog. Part. Nucl. Phys. **95**, 48 (2017), doi:10.1016/j.ppnp.2017.03.002, 1704.01356.

[2] M. Beneke *et al.*, *Top quark physics*, In *Workshop on Standard Model Physics (and more) at the LHC (First Plenary Meeting)*, pp. 419–529, doi:10.5170/CERN-2000-004.419 (2000), hep-ph/0003033.

[3] A. Jung and J. Kieseler, *Top Quarks from Tevatron to the LHC*, Symmetry **15**(10), 1915 (2023), doi:10.3390/sym15101915.

[4] P. Ferreira da Silva, *Physics of the Top Quark at the LHC: An Appraisal and Outlook of the Road Ahead*, Ann. Rev. Nucl. Part. Sci. **73**(1), 255 (2023), doi:10.1146/annurev-nucl-102419-052854.

[5] U. Baur, M. Buice and L. H. Orr, *Direct measurement of the top quark charge at hadron colliders*, Phys. Rev. D **64**, 094019 (2001), doi:10.1103/PhysRevD.64.094019, hep-ph/0106341.

[6] G. Aad *et al.*, *Measurements of inclusive and differential cross-sections of combined $t\bar{t}\gamma$ and $tW\gamma$ production in the $e\mu$ channel at 13 TeV with the ATLAS detector*, JHEP **09**, 049 (2020), doi:10.1007/JHEP09(2020)049, 2007.06946.

[7] A. Tumasyan *et al.*, *Measurement of the inclusive and differential $t\bar{t}\gamma$ cross sections in the dilepton channel and effective field theory interpretation in proton-proton collisions at $\sqrt{s}$ =13 TeV*, JHEP **05**, 091 (2022), doi:10.1007/JHEP05(2022)091, 2201.07301.

[8] M. Fael and T. Gehrmann, *Probing top quark electromagnetic dipole moments in single-top-plus-photon production*, Phys. Rev. D **88**, 033003 (2013), doi:10.1103/PhysRevD.88.033003, 1307.1349.

[9] M. Schulze and Y. Soreq, *Pinning down electroweak dipole operators of the top quark*, Eur. Phys. J. C **76**(8), 466 (2016), doi:10.1140/epjc/s10052-016-4263-x, 1603.08911.

[10] S. M. Etesami, S. Khatibi and M. Mohammadi Najafabadi, *Measuring anomalous $WW\gamma$ and $t\bar{t}\gamma$ couplings using top$+\gamma$ production at the LHC*, Eur. Phys. J. C **76**(10), 533 (2016), doi:10.1140/epjc/s10052-016-4376-2, 1606.02178.

[11] V. Khachatryan *et al.*, *Measurement of differential cross sections for top quark pair production using the lepton+jets final state in proton-proton collisions at 13 TeV*, Phys. Rev. D **95**(9), 092001 (2017), doi:10.1103/PhysRevD.95.092001, 1610.04191.

[12] M. Aaboud *et al.*, *Measurement of jet activity produced in top-quark events with an electron, a muon and two b-tagged jets in the final state in pp collisions at $\sqrt{s} = 13$ TeV with the ATLAS detector*, Eur. Phys. J. C **77**(4), 220 (2017), doi:10.1140/epjc/s10052-017-4766-0, 1610.09978.

[13] M. Aaboud *et al.*, *Measurements of differential cross sections of top quark pair production in association with jets in pp collisions at $\sqrt{s} = 13$ TeV using the ATLAS detector*, JHEP **10**, 159 (2018), doi:10.1007/JHEP10(2018)159, 1802.06572.

[14] A. M. Sirunyan *et al.*, *Measurement of the cross section for $t\bar{t}$ production with additional jets and b jets in pp collisions at $\sqrt{s} = 13$ TeV*, JHEP **07**, 125 (2020), doi:10.1007/JHEP07(2020)125, 2003.06467.

[15] A. Tumasyan *et al.*, *Differential cross section measurements for the production of top quark pairs and of additional jets using dilepton events from pp collisions at $\sqrt{s} = 13$ TeV*, JHEP **02**, 064 (2025), doi:10.1007/JHEP02(2025)064, 2402.08486.

[16] S. Alioli, P. Fernandez, J. Fuster, A. Irles, S.-O. Moch, P. Uwer and M. Vos, *A new observable to measure the top-quark mass at hadron colliders*, Eur. Phys. J. C **73**, 2438 (2013), doi:10.1140/epjc/s10052-013-2438-2, 1303.6415.

[17] G. Bevilacqua, H. B. Hartanto, M. Kraus, M. Schulze and M. Worek, *Top quark mass studies with $t\bar{t}j$ at the LHC*, JHEP **03**, 169 (2018), doi:10.1007/JHEP03(2018)169, 1710.07515.

[18] S. Alioli, J. Fuster, M. V. Garzelli, A. Gavardi, A. Irles, D. Melini, S.-O. Moch, P. Uwer and K. Voß, *Phenomenology of $t\bar{t}j + X$ production at the LHC*, JHEP **05**, 146 (2022), doi:10.1007/JHEP05(2022)146, 2202.07975.

[19] G. Aad *et al.*, *Measurement of the charge asymmetry in top-quark pair production in association with a photon with the ATLAS experiment*, Phys. Lett. B **843**, 137848 (2023), doi:10.1016/j.physletb.2023.137848, 2212.10552.

[20] S. Dittmaier, P. Uwer and S. Weinzierl, *NLO QCD corrections to t anti-t + jet production at hadron colliders*, Phys. Rev. Lett. **98**, 262002 (2007), doi:10.1103/PhysRevLett.98.262002, hep-ph/0703120.

[21] S. Alioli, S.-O. Moch and P. Uwer, *Hadronic top-quark pair-production with one jet and parton showering*, JHEP **01**, 137 (2012), doi:10.1007/JHEP01(2012)137, 1110.5251.

[22] G. Bevilacqua, H. B. Hartanto, M. Kraus and M. Worek, *Top Quark Pair Production in Association with a Jet with Next-to-Leading-Order QCD Off-Shell Effects at the Large Hadron Collider*, Phys. Rev. Lett. **116**(5), 052003 (2016), doi:10.1103/PhysRevLett.116.052003, 1509.09242.

[23] G. Bevilacqua, H. B. Hartanto, M. Kraus and M. Worek, *Off-shell Top Quarks with One Jet at the LHC: A comprehensive analysis at NLO QCD*, JHEP **11**, 098 (2016), doi:10.1007/JHEP11(2016)098, 1609.01659.

[24] C. Gütschow, J. M. Lindert and M. Schönherr, *Multi-jet merged top-pair production including electroweak corrections*, Eur. Phys. J. C **78**(4), 317 (2018), doi:10.1140/epjc/s10052-018-5804-2, 1803.00950.

[25] P.-F. Duan, W.-G. Ma, R.-Y. Zhang, L. Han, L. Guo and S.-M. Wang, *QCD corrections to associated production of $t\bar{t}\gamma$ at hadron colliders*, Phys. Rev. D **80**, 014022 (2009), doi:10.1103/PhysRevD.80.014022, 0907.1324.

[26] K. Melnikov, M. Schulze and A. Scharf, *QCD corrections to top quark pair production in association with a photon at hadron colliders*, Phys. Rev. D **83**, 074013 (2011), doi:10.1103/PhysRevD.83.074013, 1102.1967.

[27] A. Kardos and Z. Trócsányi, *Hadroproduction of t anti-t pair in association with an isolated photon at NLO accuracy matched with parton shower*, JHEP **05**, 090 (2015), doi:10.1007/JHEP05(2015)090, 1406.2324.

[28] P.-F. Duan, Y. Zhang, Y. Wang, M. Song and G. Li, *Electroweak corrections to top quark pair production in association with a hard photon at hadron colliders*, Phys. Lett. B **766**, 102 (2017), doi:10.1016/j.physletb.2016.12.061, 1612.00248.

[29] G. Bevilacqua, H. B. Hartanto, M. Kraus, T. Weber and M. Worek, *Hard Photons in Hadroproduction of Top Quarks with Realistic Final States*, JHEP **10**, 158 (2018), doi:10.1007/JHEP10(2018)158, 1803.09916.

[30] G. Bevilacqua, H. B. Hartanto, M. Kraus, T. Weber and M. Worek, *Precise predictions for $t\bar{t}\gamma/t\bar{t}$ cross section ratios at the LHC*, JHEP **01**, 188 (2019), doi:10.1007/JHEP01(2019)188, 1809.08562.

[31] G. Bevilacqua, H. B. Hartanto, M. Kraus, T. Weber and M. Worek, *Off-shell vs on-shell modelling of top quarks in photon associated production*, JHEP **03**, 154 (2020), doi:10.1007/JHEP03(2020)154, 1912.09999.

[32] D. Pagani, H.-S. Shao, I. Tsinikos and M. Zaro, *Automated EW corrections with isolated photons: $t\bar{t}\gamma$, $t\bar{t}\gamma\gamma$ and $t\gamma j$ as case studies*, JHEP **09**, 155 (2021), doi:10.1007/JHEP09(2021)155, 2106.02059.

[33] N. Kidonakis and A. Tonero, *Higher-order corrections in $t\bar{t}\gamma$ cross sections*, Phys. Rev. D **107**(3), 034013 (2023), doi:10.1103/PhysRevD.107.034013, 2212.00096.

[34] D. Stremmer and M. Worek, *Complete NLO corrections to top-quark pair production with isolated photons*, JHEP **07**, 091 (2024), doi:10.1007/JHEP07(2024)091, 2403.03796.

[35] D. Stremmer and M. Worek, *NLO QCD predictions for $t\bar{t}\gamma$ with realistic photon isolation*, JHEP **01**, 156 (2025), doi:10.1007/JHEP01(2025)156, 2411.02196.

[36] S. Badger, D. Chicherin, T. Gehrmann, G. Heinrich, J. M. Henn, T. Peraro, P. Wasser, Y. Zhang and S. Zoia, *Analytic form of the full two-loop five-gluon all-plus helicity amplitude*, Phys. Rev. Lett. **123**(7), 071601 (2019), doi:10.1103/PhysRevLett.123.071601, 1905.03733.

[37] S. Badger, H. B. Hartanto and S. Zoia, *Two-Loop QCD Corrections to $Wb\bar{b}$ Production at Hadron Colliders*, Phys. Rev. Lett. **127**(1), 012001 (2021), doi:10.1103/PhysRevLett.127.012001, 2102.02516.

[38] S. Badger, H. B. Hartanto, J. Kryś and S. Zoia, *Two-loop leading-colour QCD helicity amplitudes for Higgs boson production in association with a bottom-quark pair at the LHC*, JHEP **11**, 012 (2021), doi:10.1007/JHEP11(2021)012, 2107.14733.

[39] S. Abreu, F. Febres Cordero, H. Ita, M. Klinkert, B. Page and V. Sotnikov, *Leading-color two-loop amplitudes for four partons and a W boson in QCD*, JHEP **04**, 042 (2022), doi:10.1007/JHEP04(2022)042, 2110.07541.

[40] S. Badger, H. B. Hartanto, J. Kryś and S. Zoia, *Two-loop leading colour helicity amplitudes for $W\gamma + j$ production at the LHC*, JHEP **05**, 035 (2022), doi:10.1007/JHEP05(2022)035, 2201.04075.

[41] B. Agarwal, F. Buccioni, A. von Manteuffel and L. Tancredi, *Two-Loop Helicity Amplitudes for Diphoton Plus Jet Production in Full Color*, Phys. Rev. Lett. **127**(26), 262001 (2021), doi:10.1103/PhysRevLett.127.262001, 2105.04585.

[42] S. Badger, C. Brønnum-Hansen, D. Chicherin, T. Gehrmann, H. B. Hartanto, J. Henn, M. Marcoli, R. Moodie, T. Peraro and S. Zoia, *Virtual QCD corrections to gluon-initiated diphoton plus jet production at hadron colliders*, JHEP **11**, 083 (2021), doi:10.1007/JHEP11(2021)083, 2106.08664.

[43] S. Abreu, G. De Laurentis, H. Ita, M. Klinkert, B. Page and V. Sotnikov, *Two-loop QCD corrections for three-photon production at hadron colliders*, SciPost Phys. **15**(4), 157 (2023), doi:10.21468/SciPostPhys.15.4.157, 2305.17056.

[44] S. Badger, M. Czakon, H. B. Hartanto, R. Moodie, T. Peraro, R. Poncelet and S. Zoia, *Isolated photon production in association with a jet pair through next-to-next-to-leading order in QCD*, JHEP **10**, 071 (2023), doi:10.1007/JHEP10(2023)071, 2304.06682.

[45] B. Agarwal, F. Buccioni, F. Devoto, G. Gambuti, A. von Manteuffel and L. Tancredi, *Five-parton scattering in QCD at two loops*, Phys. Rev. D **109**(9), 094025 (2024), doi:10.1103/PhysRevD.109.094025, 2311.09870.

[46] G. De Laurentis, H. Ita, M. Klinkert and V. Sotnikov, *Double-virtual NNLO QCD corrections for five-parton scattering. I. The gluon channel*, Phys. Rev. D **109**(9), 094023 (2024), doi:10.1103/PhysRevD.109.094023, 2311.10086.

[47] G. De Laurentis, H. Ita and V. Sotnikov, *Double-virtual NNLO QCD corrections for five-parton scattering. II. The quark channels*, Phys. Rev. D **109**(9), 094024 (2024), doi:10.1103/PhysRevD.109.094024, 2311.18752.

[48] S. Badger, H. B. Hartanto, Z. Wu, Y. Zhang and S. Zoia, *Two-loop amplitudes for $\mathcal{O}\left(\alpha_s^2\right)$ corrections to $W\gamma\gamma$ production at the LHC*, JHEP **12**, 221 (2025), doi:10.1007/JHEP12(2024)221, 2409.08146.

[49] S. Badger, H. B. Hartanto, R. Poncelet, Z. Wu, Y. Zhang and S. Zoia, *Full-colour double-virtual amplitudes for associated production of a Higgs boson with a bottom-quark pair at the LHC*, JHEP **03**, 066 (2025), doi:10.1007/JHEP03(2025)066, 2412.06519.

[50] G. De Laurentis, H. Ita, B. Page and V. Sotnikov, *Compact Two-Loop QCD Corrections for Vjj Production in Proton Collisions* (2025), 2503.10595.

[51] A. von Manteuffel and R. M. Schabinger, *A novel approach to integration by parts reduction*, Phys. Lett. B **744**, 101 (2015), doi:10.1016/j.physletb.2015.03.029, 1406.4513.

[52] T. Peraro, *Scattering amplitudes over finite fields and multivariate functional reconstruction*, JHEP **12**, 030 (2016), doi:10.1007/JHEP12(2016)030, 1608.01902.

[53] F. V. Tkachov, *A theorem on analytical calculability of 4-loop renormalization group functions*, Phys. Lett. B **100**, 65 (1981), doi:10.1016/0370-2693(81)90288-4.

[54] K. G. Chetyrkin and F. V. Tkachov, *Integration by parts: The algorithm to calculate β-functions in 4 loops*, Nucl. Phys. B **192**, 159 (1981), doi:10.1016/0550-3213(81)90199-1.

[55] S. Laporta, *High-precision calculation of multiloop Feynman integrals by difference equations*, Int. J. Mod. Phys. A **15**, 5087 (2000), doi:10.1142/S0217751X00002159, hep-ph/0102033.

[56] G. Barucchi and G. Ponzano, *Differential equations for one-loop generalized feynman integrals*, J. Math. Phys. **14**, 396 (1973), doi:10.1063/1.1666327.

[57] A. V. Kotikov, *Differential equations method: New technique for massive Feynman diagrams calculation*, Phys. Lett. B **254**, 158 (1991), doi:10.1016/0370-2693(91)90413-K.

[58] A. V. Kotikov, *Differential equations method: The Calculation of vertex type Feynman diagrams*, Phys. Lett. B **259**, 314 (1991), doi:10.1016/0370-2693(91)90834-D.

[59] Z. Bern, L. J. Dixon and D. A. Kosower, *Dimensionally regulated pentagon integrals*, Nucl. Phys. B **412**, 751 (1994), doi:10.1016/0550-3213(94)90398-0, hep-ph/9306240.

[60] T. Gehrmann and E. Remiddi, *Differential equations for two-loop four-point functions*, Nucl. Phys. B **580**, 485 (2000), doi:10.1016/S0550-3213(00)00223-6, hep-ph/9912329.

[61] J. M. Henn, *Multiloop integrals in dimensional regularization made simple*, Phys. Rev. Lett. **110**, 251601 (2013), doi:10.1103/PhysRevLett.110.251601, 1304.1806.

[62] T. Gehrmann, J. M. Henn and N. A. Lo Presti, *Pentagon functions for massless planar scattering amplitudes*, JHEP **10**, 103 (2018), doi:10.1007/JHEP10(2018)103, 1807.09812.

[63] D. Chicherin and V. Sotnikov, *Pentagon Functions for Scattering of Five Massless Particles*, JHEP **20**, 167 (2020), doi:10.1007/JHEP12(2020)167, 2009.07803.

[64] D. Chicherin, V. Sotnikov and S. Zoia, *Pentagon functions for one-mass planar scattering amplitudes*, JHEP **01**, 096 (2022), doi:10.1007/JHEP01(2022)096, 2110.10111.

[65] S. Badger, M. Becchetti, E. Chaubey and R. Marzucca, *Two-loop master integrals for a planar topology contributing to $pp \rightarrow t\bar{t}j$*, JHEP **01**, 156 (2023), doi:10.1007/JHEP01(2023)156, 2210.17477.

[66] S. Badger, M. Becchetti, N. Giraudo and S. Zoia, *Two-loop integrals for $t\bar{t}$+jet production at hadron colliders in the leading colour approximation*, JHEP **07**, 073 (2024), doi:10.1007/JHEP07(2024)073, 2404.12325.

[67] M. Becchetti, C. Dlapa and S. Zoia, *Canonical differential equations for the elliptic two-loop five-point integral family relevant to $t\bar{t}$+jet production at leading colour* (2025), 2503.03603.

[68] F. Febres Cordero, G. Figueiredo, M. Kraus, B. Page and L. Reina, *Two-loop master integrals for leading-color $pp \rightarrow t\bar{t}H$ amplitudes with a light-quark loop*, JHEP **07**, 084 (2024), doi:10.1007/JHEP07(2024)084, 2312.08131.

[69] M. Becchetti, D. Canko, V. Chestnov, T. Peraro, M. Pozzoli and S. Zoia, *Two-loop Feynman integrals for leading colour $t\bar{t}W$ production at hadron colliders* (2025), 2504.13011.

[70] S. Badger, M. Becchetti, C. Brancaccio, H. B. Hartanto and S. Zoia, *Numerical evaluation of two-loop QCD helicity amplitudes for $gg \rightarrow t\bar{t}g$ at leading colour*, JHEP **03**, 070 (2025), doi:10.1007/JHEP03(2025)070, 2412.13876.

[71] B. Agarwal, G. Heinrich, S. P. Jones, M. Kerner, S. Y. Klein, J. Lang, V. Magerya and A. Olsson, *Two-loop amplitudes for $t\bar{t}H$ production: the quark-initiated N_f-part*, JHEP **05**, 013 (2024), doi:10.1007/JHEP05(2024)013, [Erratum: JHEP 06, 142 (2024)], 2402.03301.

[72] J. Alwall, R. Frederix, S. Frixione, V. Hirschi, F. Maltoni, O. Mattelaer, H. S. Shao, T. Stelzer, P. Torrielli and M. Zaro, *The automated computation of tree-level and next-to-leading order differential cross sections, and their matching to parton shower simulations*, JHEP **07**, 079 (2014), doi:10.1007/JHEP07(2014)079, 1405.0301.

[73] G. Bevilacqua, M. Czakon, M. V. Garzelli, A. van Hameren, A. Kardos, C. G. Papadopoulos, R. Pittau and M. Worek, *HELAC-NLO*, Comput. Phys. Commun. **184**, 986 (2013), doi:10.1016/j.cpc.2012.10.033, 1110.1499.

[74] G. Cullen *et al.*, *GOSAM-2.0: a tool for automated one-loop calculations within the Standard Model and beyond*, Eur. Phys. J. C **74**(8), 3001 (2014), doi:10.1140/epjc/s10052-014-3001-5, 1404.7096.

[75] A. Denner, J.-N. Lang and S. Uccirati, *Recola2: REcursive Computation of One-Loop Amplitudes 2*, Comput. Phys. Commun. **224**, 346 (2018), doi:10.1016/j.cpc.2017.11.013, 1711.07388.

[76] F. Buccioni, J.-N. Lang, J. M. Lindert, P. Maierhöfer, S. Pozzorini, H. Zhang and M. F. Zoller, *OpenLoops 2*, Eur. Phys. J. C **79**(10), 866 (2019), doi:10.1140/epjc/s10052-019-7306-2, 1907.13071.

[77] S. Badger, M. Becchetti, E. Chaubey, R. Marzucca and F. Sarandrea, *One-loop QCD helicity amplitudes for $pp \to t\bar{t}j$ to $O(\varepsilon^2)$*, JHEP **06**, 066 (2022), doi:10.1007/JHEP06(2022)066, 2201.12188.

[78] F. Buccioni, P. A. Kreer, X. Liu and L. Tancredi, *One loop QCD corrections to $gg \to t\bar{t}H$ at $\mathcal{O}(\epsilon^2)$*, JHEP **03**, 093 (2024), doi:10.1007/JHEP03(2024)093, 2312.10015.

[79] M. Becchetti, M. Delto, S. Ditsch, P. A. Kreer, M. Pozzoli and L. Tancredi, *One-Loop QCD Corrections to $\bar{u}d \to t\bar{t}W$ at $\mathcal{O}(\varepsilon^2)$* (2025), 2502.14952.

[80] S. Pozzorini and E. Remiddi, *Precise numerical evaluation of the two loop sunrise graph master integrals in the equal mass case*, Comput. Phys. Commun. **175**, 381 (2006), doi:10.1016/j.cpc.2006.05.005, hep-ph/0505041.

[81] F. Moriello, *Generalised power series expansions for the elliptic planar families of Higgs + jet production at two loops*, JHEP **01**, 150 (2020), doi:10.1007/JHEP01(2020)150, 1907.13234.

[82] M. Hidding, *DiffExp, a Mathematica package for computing Feynman integrals in terms of one-dimensional series expansions*, Comput. Phys. Commun. **269**, 108125 (2021), doi:10.1016/j.cpc.2021.108125, 2006.05510.

[83] R. M. Prisco, J. Ronca and F. Tramontano, *LINE: Loop Integrals Numerical Evaluation* (2025), 2501.01943.

[84] T. Peraro, *FiniteFlow: multivariate functional reconstruction using finite fields and dataflow graphs*, JHEP **07**, 031 (2019), doi:10.1007/JHEP07(2019)031, 1905.08019.

[85] T. Peraro and L. Tancredi, *Physical projectors for multi-leg helicity amplitudes*, JHEP **07**, 114 (2019), doi:10.1007/JHEP07(2019)114, 1906.03298.

[86] T. Peraro and L. Tancredi, *Tensor decomposition for bosonic and fermionic scattering amplitudes*, Phys. Rev. D **103**(5), 054042 (2021), doi:10.1103/PhysRevD.103.054042, 2012.00820.

[87] R. Kleiss and W. J. Stirling, *Spinor Techniques for Calculating p anti-p —> W+- / Z0 + Jets*, Nucl. Phys. B **262**, 235 (1985), doi:10.1016/0550-3213(85)90285-8.

[88] S. Badger, E. Chaubey, H. B. Hartanto and R. Marzucca, *Two-loop leading colour QCD helicity amplitudes for top quark pair production in the gluon fusion channel*, JHEP **06**, 163 (2021), doi:10.1007/JHEP06(2021)163, 2102.13450.

[89] N. Arkani-Hamed, T.-C. Huang and Y.-t. Huang, *Scattering amplitudes for all masses and spins*, JHEP **11**, 070 (2021), doi:10.1007/JHEP11(2021)070, 1709.04891.

[90] P. Nogueira, *Automatic Feynman Graph Generation*, J. Comput. Phys. **105**, 279 (1993), doi:10.1006/jcph.1993.1074.

[91] B. Ruijl, T. Ueda and J. Vermaseren, *FORM version 4.2* (2017), 1707.06453.

[92] Z. Wu, J. Boehm, R. Ma, H. Xu and Y. Zhang, *NeatIBP 1.0, a package generating small-size integration-by-parts relations for Feynman integrals*, Comput. Phys. Commun. **295**, 108999 (2024), doi:10.1016/j.cpc.2023.108999, 2305.08783.

[93] A. Hodges, *Eliminating spurious poles from gauge-theoretic amplitudes*, JHEP **05**, 135 (2013), doi:10.1007/JHEP05(2013)135, 0905.1473.

[94] S. Badger, *Automating QCD amplitudes with on-shell methods*, J. Phys. Conf. Ser. **762**(1), 012057 (2016), doi:10.1088/1742-6596/762/1/012057, 1605.02172.

[95] T. Becher and M. Neubert, *Infrared singularities of scattering amplitudes in perturbative QCD*, Phys. Rev. Lett. **102**, 162001 (2009), doi:10.1103/PhysRevLett.102.162001, [Erratum: Phys.Rev.Lett. 111, 199905 (2013)], 0901.0722.

[96] T. Becher and M. Neubert, *On the Structure of Infrared Singularities of Gauge-Theory Amplitudes*, JHEP **06**, 081 (2009), doi:10.1088/1126-6708/2009/06/081, [Erratum: JHEP 11, 024 (2013)], 0903.1126.

[97] T. Becher and M. Neubert, *Infrared singularities of QCD amplitudes with massive partons*, Phys. Rev. D **79**, 125004 (2009), doi:10.1103/PhysRevD.79.125004, [Erratum: Phys.Rev.D 80, 109901 (2009)], 0904.1021.

[98] E. Gardi and L. Magnea, *Factorization constraints for soft anomalous dimensions in QCD scattering amplitudes*, JHEP **03**, 079 (2009), doi:10.1088/1126-6708/2009/03/079, 0901.1091.

[99] E. Gardi and L. Magnea, *Infrared singularities in QCD amplitudes*, Nuovo Cim. C **32N5-6**, 137 (2009), doi:10.1393/ncc/i2010-10528-x, 0908.3273.

[100] S. Catani, S. Dittmaier and Z. Trocsanyi, *One loop singular behavior of QCD and SUSY QCD amplitudes with massive partons*, Phys. Lett. B **500**, 149 (2001), doi:10.1016/S0370-2693(01)00065-X, hep-ph/0011222.

[101] A. Ferroglia, M. Neubert, B. D. Pecjak and L. L. Yang, *Two-loop divergences of massive scattering amplitudes in non-abelian gauge theories*, JHEP **11**, 062 (2009), doi:10.1088/1126-6708/2009/11/062, 0908.3676.

[102] S. Bera, C. Brancaccio, D. Canko and H. B. Hartanto, *Ancillary files for "One-loop amplitudes for $t\bar{t}j$ and $t\bar{t}\gamma$ productions at the LHC through $\mathcal{O}(\epsilon^2)$"*, doi:10.5281/zenodo.15398292 (2025).

[103] M. Heller and A. von Manteuffel, *MultivariateApart: Generalized partial fractions*, Comput. Phys. Commun. **271**, 108174 (2022), doi:10.1016/j.cpc.2021.108174, 2101.08283.

[104] S. Abreu, D. Chicherin, H. Ita, B. Page, V. Sotnikov, W. Tschernow and S. Zoia, *All Two-Loop Feynman Integrals for Five-Point One-Mass Scattering*, Phys. Rev. Lett. **132**(14), 141601 (2024), doi:10.1103/PhysRevLett.132.141601, 2306.15431.

[105] C. Brancaccio, *Towards two-loop QCD corrections to* **pp → t̄tj**, In *17th International Workshop on Top Quark Physics* (2024), 2411.10856.

[106] R. N. Lee, *LiteRed 1.4: a powerful tool for reduction of multiloop integrals*, J. Phys. Conf. Ser. **523**, 012059 (2014), doi:10.1088/1742-6596/523/1/012059, 1310.1145.

[107] S. Badger, J. Kryś, R. Moodie and S. Zoia, *Lepton-pair scattering with an off-shell and an on-shell photon at two loops in massless QED*, JHEP **11**, 041 (2023), doi:10.1007/JHEP11(2023)041, 2307.03098.

[108] A. A H, E. Chaubey and H.-S. Shao, *Two-loop massive QCD and QED helicity amplitudes for light-by-light scattering*, JHEP **03**, 121 (2024), doi:10.1007/JHEP03(2024)121, 2312.16966.

[109] T. Gehrmann, J. Henn, P. Jakubčík, J. Lim, C. C. Mella, N. Syrrakos, L. Tancredi and W. J. Torres Bobadilla, *Graded transcendental functions: an application to four-point amplitudes with one off-shell leg* (2024), 2410.19088.

[110] X. Liu and Y.-Q. Ma, *AMFlow: A Mathematica package for Feynman integrals computation via auxiliary mass flow*, Comput. Phys. Commun. **283**, 108565 (2023), doi:10.1016/j.cpc.2022.108565, 2201.11669.

[111] X. Liu, Y.-Q. Ma and C.-Y. Wang, *A Systematic and Efficient Method to Compute Multi-loop Master Integrals*, Phys. Lett. B **779**, 353 (2018), doi:10.1016/j.physletb.2018.02.026, 1711.09572.

[112] K.-T. Chen, *Iterated path integrals*, Bull. Am. Math. Soc. **83**, 831 (1977), doi:10.1090/S0002-9904-1977-14320-6.

[113] A. B. Goncharov, *Galois symmetries of fundamental groupoids and noncommutative geometry*, Duke Math. J. **128**, 209 (2005), doi:10.1215/S0012-7094-04-12822-2, math/0208144.

[114] A. B. Goncharov, *A simple construction of Grassmannian polylogarithms* (2009), 0908.2238.

[115] C. Duhr, H. Gangl and J. R. Rhodes, *From polygons and symbols to polylogarithmic functions*, JHEP **10**, 075 (2012), doi:10.1007/JHEP10(2012)075, 1110.0458.

[116] N. Byers and C. N. Yang, *Physical Regions in Invariant Variables for n Particles and the Phase-Space Volume Element*, Rev. Mod. Phys. **36**(2), 595 (1964), doi:10.1103/RevModPhys.36.595.

[117] E. Byckling and K. Kajantie, *Particle Kinematics: (Chapters I-VI, X)*, University of Jyvaskyla, Jyvaskyla, Finland (1971).

[118] S. Caron-Huot and J. M. Henn, *Iterative structure of finite loop integrals*, JHEP **06**, 114 (2014), doi:10.1007/JHEP06(2014)114, 1404.2922.

[119] K. Melnikov and T. van Ritbergen, *The Three loop on-shell renormalization of QCD and QED*, Nucl. Phys. B **591**, 515 (2000), doi:10.1016/S0550-3213(00)00526-5, hep-ph/0005131.

[120] R. Bonciani, A. Ferroglia, T. Gehrmann, A. von Manteuffel and C. Studerus, *Two-Loop Leading Color Corrections to Heavy-Quark Pair Production in the Gluon Fusion Channel*, JHEP **01**, 102 (2011), doi:10.1007/JHEP01(2011)102, 1011.6661.